ORNL/TM-2022/1844

# Application of SCALE to Molten Salt Fueled Reactor Physics in Support of Severe Accident Analyses


Austin Lo
Friederike Bostelmann
Donny Hartanto
Benjamin R. Betzler
William A. Wieselquist



**November 1, 2022**

OAK RIDGE National Laboratory

ORNL IS MANAGED BY UT–BATTELLE, LLC, FOR THE U.S. DEPARTMENT OF ENERGY

**ORNL/TM-2022/1844**

Nuclear Energy and Fuel Cycle Division

# APPLICATION OF SCALE TO MOLTEN SALT FUELED REACTOR PHYSICS IN SUPPORT OF SEVERE ACCIDENT ANALYSES

Austin Lo
Friederike Bostelmann
Donny Hartanto
Benjamin R. Betzler
William A. Wieselquist

Date Published: November 1, 2022

Prepared by
OAK RIDGE NATIONAL LABORATORY
Oak Ridge, TN 37831-6283
managed by
UT-Battelle, LLC
for the
US DEPARTMENT OF ENERGY
under contract DE-AC05-00OR22725

## CONTENTS

## LIST OF FIGURES

## LIST OF TABLES

## ABBREVIATIONS

| | |
|---|---|
| ARE | Aircraft Reactor Experiment |
| DNP | delayed neutron precursor |
| FHR | fluoride salt-cooled high-temperature reactor |
| HX | heat exchanger |
| IRPhEP | International Reactor Physics Experiment Evaluation Project |
| LWR | light-water reactor |
| MSR | molten salt-fueled reactor |
| MSRE | Molten Salt Reactor Experiment |
| MTIHM | metric ton initial heavy metal |
| NRC | US Nuclear Regulatory Commission |
| ODE | ordinary differential equation |
| OGS | off gas system |
| ORIGEN | Oak Ridge Isotope Generation code |
| ORNL | Oak Ridge National Laboratory |
| PF | poison fraction |
| SNL | Sandia National Laboratories |
| UCB | University of California, Berkeley |

## ACKNOWLEDGMENTS

Support for this work was provided by the US Nuclear Regulatory Commission (NRC) under Contract IAA 31310019N0012. The authors would especially like to thank program managers Don Algama and Lucas Kyriazidis of the NRC for their support and constructive feedback. Suggestions and comments received from many of our colleagues in ORNL's Nuclear Energy and Fuel Cycle Division are greatly appreciated. The feedback provided by the MELCOR team, in particular from K.C. Wagner (Sandia National Laboratories), David L. Luxat (Sandia National Laboratories), and Jason Schaperow (NRC) was very helpful.

## ABSTRACT

As part of a US Nuclear Regulatory Commission–sponsored project to assess the modeling and simulation capabilities for accident progression, source term, and consequence analysis for advanced reactor technologies with SCALE and MELCOR, SCALE was used for the modeling and simulation of a molten salt-fueled reactor (MSR).

SCALE capabilities for the modeling of MSR physics were demonstrated based on the Molten Salt Reactor Experiment (MSRE). Of primary interest were the determination of the system's nuclide inventory, as well as the inventories in the various regions of the loop, considering that the fuel is continuously pumped through the system. This report contains discussions on the following:

1. Determination of the system-average fuel salt inventory considering fission gas removal in the off-gas system and noble metal removal through plating out at the heat exchanger using recent enhancements in SCALE's depletion sequence TRITON,
2. Assessment of the nuclide spatial distribution throughout the loop using SCALE's depletion solver ORIGEN,
3. Calculation of the core's power profile, flux profile, temperature reactivity coefficients, and xenon reactivity using full-core calculations with SCALE's Monte Carlo code KENO-VI.

The results obtained with SCALE were post-processed to provide the MELCOR team with the core inventory and decay heat of the system, as well as the inventory and decay heat of individual regions in the loop, a zone-wise power profile, temperature feedback coefficients, and the xenon worth.

# 1. INTRODUCTION

To assess the modeling and simulation capabilities for accident progression, source term, and consequence analysis for non-light-water reactor (LWR) technologies, the US Nuclear Regulatory Commission (NRC) initiated a collaborative project between the NRC, Sandia National Laboratories (SNL), and Oak Ridge National Laboratory (ORNL) [1]. The SNL team is continuing to develop and use the computer code MELCOR [2] to perform severe accident progression and source term analyses. For these analyses, the ORNL team provides fission product and radionuclide inventories, kinetics parameters, power distributions, and decay heat as determined with SCALE. Following the reports about SCALE methods and analysis results of the pebble-bed HTGR PBMR-400 [3], the INL A heat pipe reactor [4], and a pebble-bed fluoride salt-cooled high-temperature reactor (FHR) [5], this report summarizes the application of SCALE for the analysis of a molten salt-fueled reactor (MSR).

## 1.1 MOLTEN SALT REACTORS

MSRs may be grouped into two subcategories: molten salt *fueled* reactors, which are characterized by the molten salt-fluidic nature of the fuel itself, and molten salt *cooled* reactors, which use a molten salt coolant for heat transfer from a solid state fuel (e.g., the FHR). The subject of this report is the molten salt *fueled* reactor, referred to simply as an MSRs from now on.

As mentioned above, the fuel's liquid state is fundamentally unique to MSR technology. During operation, the fuel salt flows in a circuitous route into and out of the active region of the reactor core. While MSRs may be designed neutronically to have either a thermal or fast neutron spectrum, the focus of this study is on the former. Molten salt fuels have the unique ability to carry out fuel processing *in situ* and *during* normal power operations. Benefits associated with liquid fuels are lower fuel fabrication, handling, and reprocessing costs; improved fuel cycle performance; and increased safety. The primary concern associated with liquid fuels is radionuclide accountability as it pertains to increased proliferation and primary containment risks.

## 1.2 US EXPERIENCE WITH MSRS

The majority of US-based experimental work in MSR technology has been performed at ORNL and can be grouped into two distinct, sequential efforts: the Aircraft Reactor Experiment (ARE) and the MSRE [6]. MSRs were initially pursued to provide compact, high-temperature heat for aircraft propulsion for long-duration defense-based mission sets. Although the successful operation of a 2.5 MWth reactor was encouraging for this application, its integration into a flight-worthy system proved to be more challenging (and costly); furthermore, the advent of the intercontinental ballistic missile in 1959 essentially eliminated any need for nuclear-powered aircraft as a strategic deterrent. Defense applications gave way to civil applications, and the prospect of using MSR technology for low-cost, grid-scale power generation gave rise to the MSRE, whose campaign spanned from 1965 (initial criticality) to 1969. The MSRE campaign achieved its primary goal in demonstrating practicality for grid-scale power generation, but it was eventually abandoned at the end of its campaign and was not revisited seriously until half a century later.

Despite the capricious termination of the program, MSRE provides one of the most extensive experimental databases for the MSR class, which has attracted broad attention from multiple public and private entities. These entities have reinvigorated the need for MSRs and are developing the technology toward commercialization for grid-scale power [7].

## 1.3 PREVIOUS MSR SIMULATION EFFORTS

Coinciding with the recent MSR technology revitalization efforts, modeling and simulation efforts for MSR have also progressed. While many published reports describe different experiments associated with the MSRE, and many computational analyses have been performed for different areas of interest, at this writing, only a few documents about reactor physics assessment of the MSRE have been published. Recently, University of California, Berkeley (UCB) and ORNL collaborated to develop the MSR-related reactor physics benchmark based on a series of zero-power experiments conducted at the MSRE [8]. The study assumed use of a fresh fuel salt, and it accounted for only one specific nuclide spatial effect which is necessary to model reactivity effects: delayed neutron precursor drift. Fission products that emit delayed neutrons are called delayed neutron precursors (DNPs). In flowing fuel systems, the fuel with all fission products, including the DNPs, is leaving the core so that delayed neutrons from DNPs may be born outside of the core. This DNP drift impacts reactivity control, and it is dependent on the flow rate. To model DNP drift, the MSRE benchmark uses an assumed power profile in combination with a neutron decay probability model, which accounts for the number of neutrons produced DNP *out of* the core. This yields $\beta_{\text{eff}}$, which is then used in the calculation of reactivity effects. The benchmark was successfully reviewed by the International Reactor Physics Experiment Evaluation Project (IRPhEP) committee and is available in the IRPhEP handbook beginning with the 2019 edition. The IRPhEP benchmark provides the experimental eigenvalue and the corresponding experimental uncertainty. The benchmark also includes a calculated eigenvalue and documents a first assessment of the influence of nuclear data uncertainties on the eigenvalue, which is also published in the open literature [8, 9, 10].

Over the last couple of years, the SCALE code system [11] was further developed for the modeling and simulation of MSRs, and various MSR studies were performed with different objectives. Recent enhancements to SCALE's TRITON depletion sequence for MSR analysis, often referred to as *TRITON-MSR*, [12, 13], allow for the consideration of continuous feed of nuclides into mixtures (e.g., to simulate refueling with $^{235}$U), and fractional removal of nuclides from mixtures (e.g., to simulate noble gas removal). This approach enables studies with realistic approximation of fuel salt inventory [14, 15, 16]. A worthwhile study is the analysis of reactivity change due to DNP drift. This analysis was performed using the SCALE's deterministic transport solver NEWT [12]. SCALE's uncertainty analysis tool Sampler allowed for investigations of the impact of uncertainties in an MSR's design's range on key operational parameters [17]. Simulation of the spatially dependent composition of the fuel salt as it passes through the core and primary loop was realized by application of SCALE's depletion solver ORIGEN [18]. Based on the described MSRE IRPhEP benchmark, SCALE was recently used for criticality calculations and an assessment of the impact of different nuclear data libraries and cross section uncertainties on the MSRE's criticality [19]. The SCALE full-core MSRE model developed for this study, as illustrated in Figures 1 through 3, provides the basis for the modeling work described in this report.

## 1.4 APPROACH

Given that both the benefits and concerns on MSR technology center on the fuel's flowing nature, it is desirable to capture consequent effects on reactor physics and nuclide inventories. Namely, it is of interest to model nuclide spatial distribution alterations caused by fuel flow and the fuel's composition change resulting from nuclide removal (or addition). These effects have been broadly grouped into *system-average* and *spatial* (along the dimension of the fuel loop) effects. This approach to modeling these effects may be grouped into three separate models using the SCALE code system:

1. 2D TRITON axial core slice depletion to determine system-average nuclide inventory, and corresponding ORIGEN cross-section libraries at various points in time,

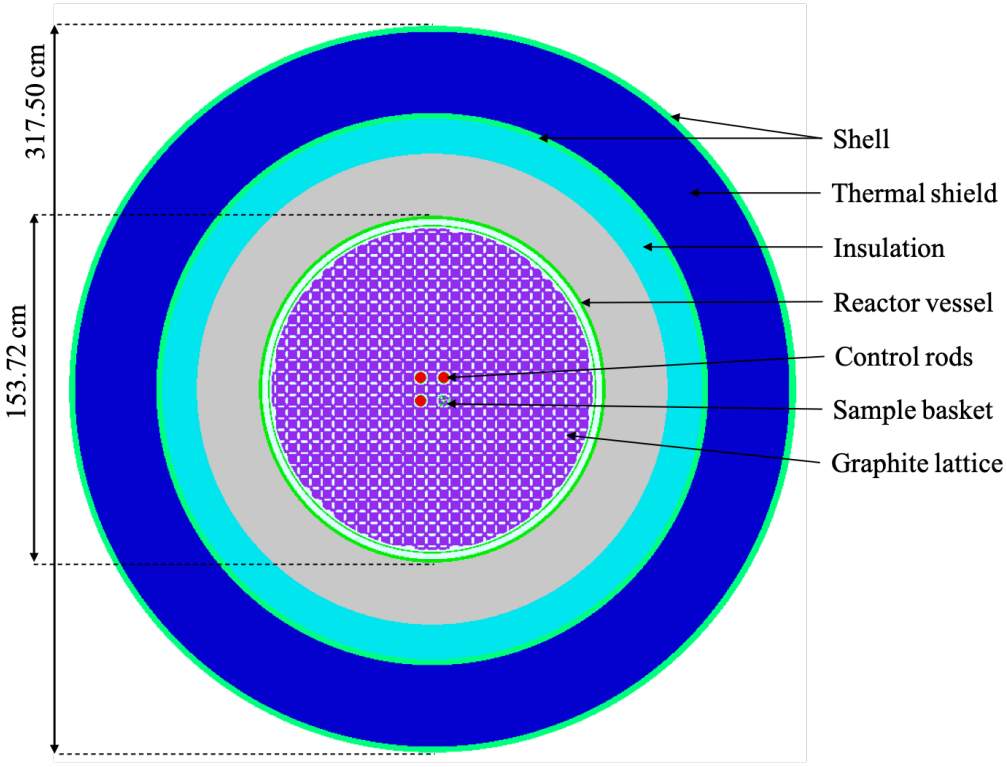


**Figure 1. Horizontal cut through the SCALE 3D MSRE core model [19].**

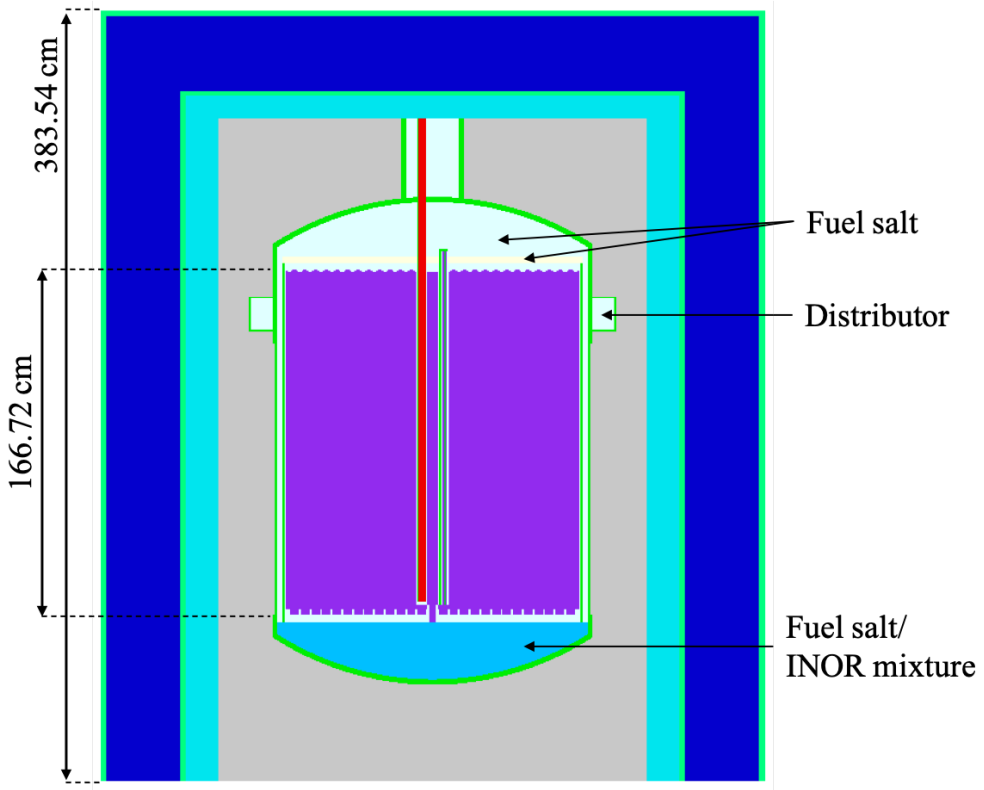


**Figure 2. Axial cut through the SCALE 3D MSRE core model [19].**

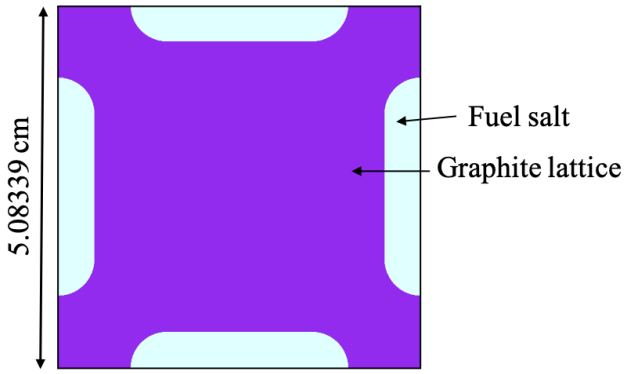


**Figure 3. Unit cell of the SCALE MSRE model [19].**

2. 3D Monte Carlo full core calculations to calculate 3D core power and flux distributions at a single point in time, and
3. 1D ORIGEN system loop calculations to determine spatially dependent nuclide inventory throughout the system.

Numerous studies treat flowing fuel effects on both a system- and spatial-level basis using state-of-the-art reactor physics tools. However, none have offered a method or framework to model these two disparate timescales *in tandem*: therefore, this is primary objective of this study.

All calculations were performed using SCALE 6.3 [20] in combination with ENDF/B-VII.1 nuclear data libraries [21] on an ORNL Linux cluster of Intel(R) Xeon(R) Gold 5118 CPUs running at 2.3 GHz. A collection of SCALE input and output files, including those developed for the MSRE, are provided in the public SCALE model repository associated with this project at `https://code.ornl.gov/scale/analysis/non-lwr-models-vol3`.

The results obtained with SCALE were post-processed to initialize MELCOR with the core inventory and decay heat of the equilibrium core, a spatially discretized power profile, temperature feedback coefficients, and removal rates for various element groups in the off-gas system and through plating out.

### 1.5 REPORT STRUCTURE

The remainder of this report is organized as follows: Section 2 provides a description of the MSRE, and Section 3 describes the approaches applied in this study. The analyses of the axial core slice, 3D full core, and 1D system loop are discussed in Sections 4, 5, and 6, respectively. Finally, Section 7 presents conclusions and recommendations for future work.

## 2. MOLTEN SALT REACTOR EXPERIMENT

The MSRE was the first large-scale, long-term, high-temperature experiment performed using a fluid fuel salt, a graphite moderator, and new nickel-based alloys in a reactor environment. The circulating fuel was a mixture of lithium, beryllium, and zirconium fluoride salts containing uranium fluorides. Reactor heat was transferred from the fuel salt to a coolant salt and was then dissipated to the atmosphere. The MSRE was designed to provide a thermal output of 10 MWth. The reactor reached criticality for the first time in June of 1965. The MSRE was initially operated using $^{235}$U, and was later switched to $^{233}$U. The present work focuses on the MSRE with $^{235}$U, considering that the MSRE was operated with $^{235}$U for 9,006 equivalent full-power hours [22].

The studies presented in this report required detailed information about the MSRE core for the generation of a 3D full core model and information about the loop to estimate the fuel salt composition during operation.

### 2.1 CORE

A detailed description of the MSRE core is provided in the IRPhEP handbook [23] for the zero-power first critical experiment with $^{235}$U, and a brief summary is presented herein. Table 1 presents an overview of the MSRE's key characteristics, and Figures 4 and 5 are illustrations of the reactor core.

The MSRE core consisted of a lattice of rectangular prism-shaped graphite "stringers" that were vertically oriented within a cylindrical reactor vessel and through which the salt was pumped in upward direction. Each vertical graphite stringer had a side length of 5.08 cm and an axial length of 170.31 cm. The salt flowed through more than 1,000 channels. Each channel was ~1 cm thick and was formed by grooves in the sides of the stringers (Figure 6). Each groove consisted of a rounded rectangle that was 4.064 cm wide with a corner radius of 0.508 mm. In the center of the core, three graphite sample baskets were mounted to allow for investigation of the graphite moderator's behavior in the reactor environment through periodic removals of graphite specimens.

The salt served the dual purpose of carrying the fuel and cooling the core. It was composed of (1) the carrier salt containing the beryllium, zirconium, and most of the lithium fluorides, (2) depleted uranium eutectic (73LiF-27$UF_4$), and (3) highly enriched uranium eutectic (73LiF-27$UF_4$). The reactor vessel consisted of INOR-8, a nickel-based alloy. The core was surrounded by an insulator, simplified in the benchmark specification as a homogeneous mixture (O, Fe, Al, H, Si, Ca), and a steel thermal shield.

The benchmark specifications assumed the temperature of the thermal shield and insulation as 305 K based on the assumption that the temperature of these components are the same as for the water that is passing through the thermal shield; the temperature for all other materials was 911 K.

### 2.2 LOOP

Figure 7 indicates the individual regions of the loop through which the salt travels during operation. The fuel salt entered the flow distributor at the top of the vessel through the fuel inlet (region 8). The fuel salt was then distributed evenly around the circumference of the vessel, and then it flowed downward through a ~2.54 cm annulus between the vessel wall and the core can into the lower head (region 9). The salt was then pumped upward through the graphite lattice (region 1) to reach the upper head of the vessel (region 2). The salt was then pumped to the OGS (region 4) before entering the HX (region 6) and being returned to the core. Table 2 provides the residence time and the salt volumes in the individual regions.

**Table 1. Key characteristics of the MSRE [23]**

| | |
|---|---|
| **General characteristics** | |
| Reactor power (MWth) | 10[a]/ 8[b] |
| Fuel salt density (g/cm$^3$) | 2.3275 |
| Graphite density (g/cm$^3$) | 1.8507 |
| Fuel and coolant composition (expressed as molar percent) | 64.88 LiF<br>29.27 $BeF_2$<br>5.06 $ZrF_4$<br>0.79 $UF_4$ |
| **Core dimensions** | |
| Graphite lattice radius (cm) | 780.285 |
| Inner core can radius (cm) | 71.097 |
| Outer core can radius (cm) | 71.737 |
| Inner reactor vessel radius (cm) | 74.299 |
| Outer reactor vessel (inactive region) radius (cm) | 75.741 |
| Height of the core can (cm) | 174.219 |
| Total height of the vessel (from the vessel bottom to the top of outlet pipe) (cm) | 272.113 |
| **Graphite stringer characteristics** | |
| Individual stringer width (cm) | 5.084 |
| Fuel channel thickness (cm) | 1.018 |
| Fuel channel width (cm) | 3.053 |
| Cutout radius at fuel channel corners (mm) | 0.508 |
| Graphite stringer height (cm) | 170.311 |

[a] initial criticality
[b] during operation

**Table 2. MSRE loop details [24]**

| Region | Description | Salt volume (m$^3$) | Residence time (s) | $^{235}$U Mass (kg) |
|---|---|---|---|---|
| 1 | Core | 0.708 | 9.4 | 77.3 |
| 2 | Upper plenum | 0.297 | 3.9 | 32.5 |
| 3 | Reactor to pump | 0.059 | 0.8 | 6.5 |
| 4 | Pump | 0.116 | 0.3 | 12.7 |
| 5 | Pump to heat exchanger | 0.023 | 0.3 | 2.5 |
| 6 | Heat exchanger | 0.173 | 2.3 | 18.9 |
| 7 | Heat exchanger to inlet | 0.062 | 0.8 | 6.8 |
| 8 | Inlet | 0.275 | 3.6 | 30.0 |
| 9 | Lower plenum | 0.283 | 3.8 | 30.9 |
| | **System total** | **1.996** | **25.2** | **218** |

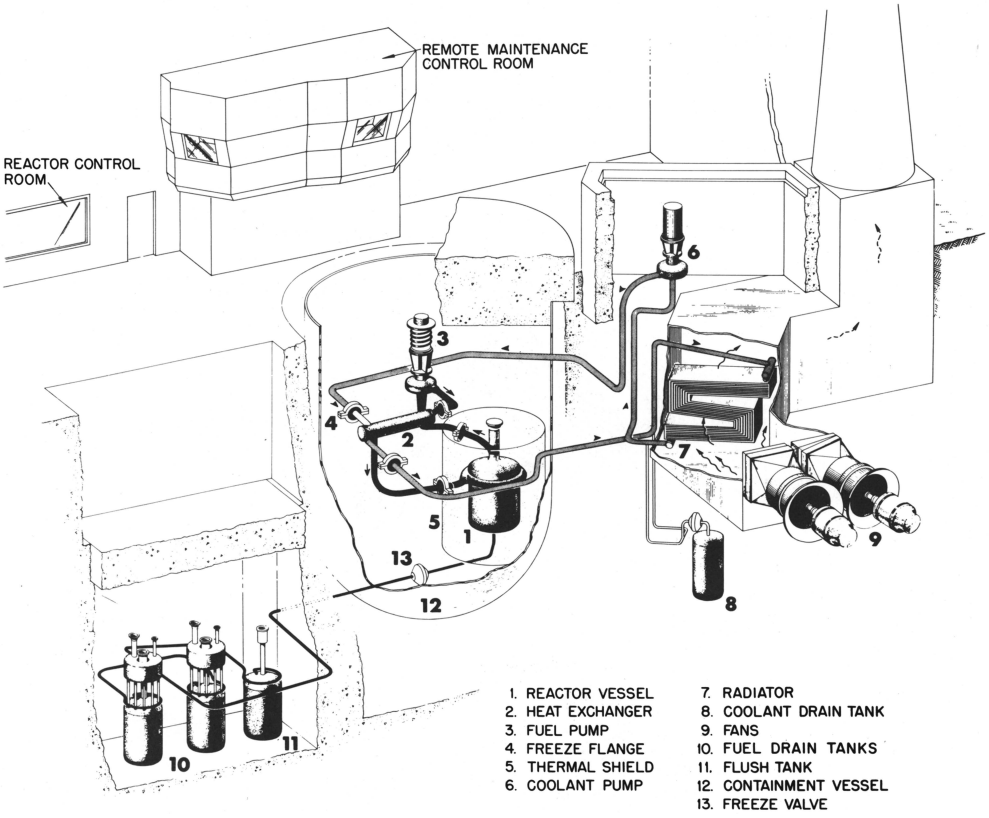


**Figure 4. MSRE layout [22, 24].**

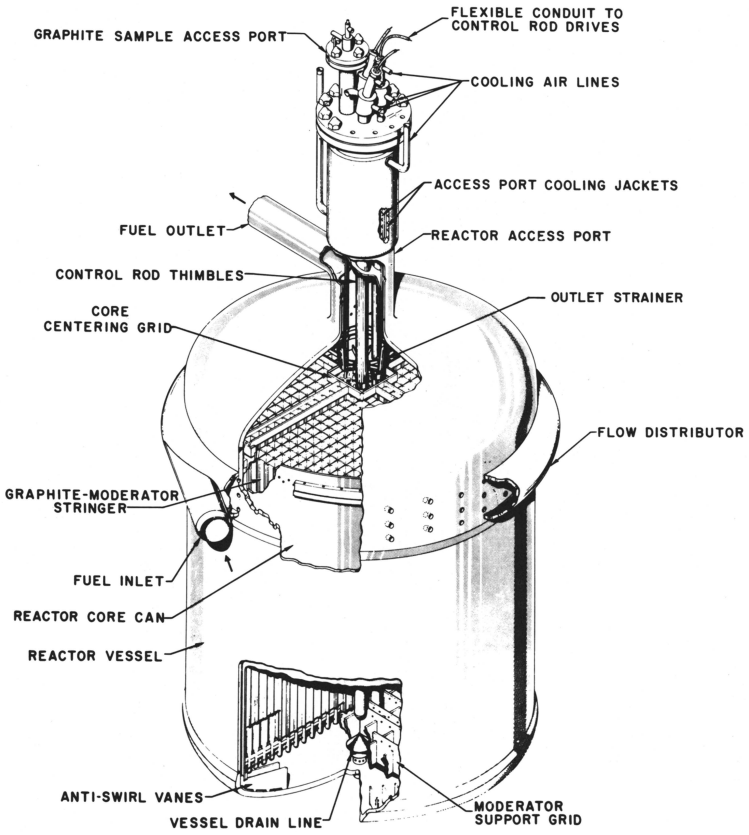


**Figure 5. MSRE reactor vessel [22, 24].**

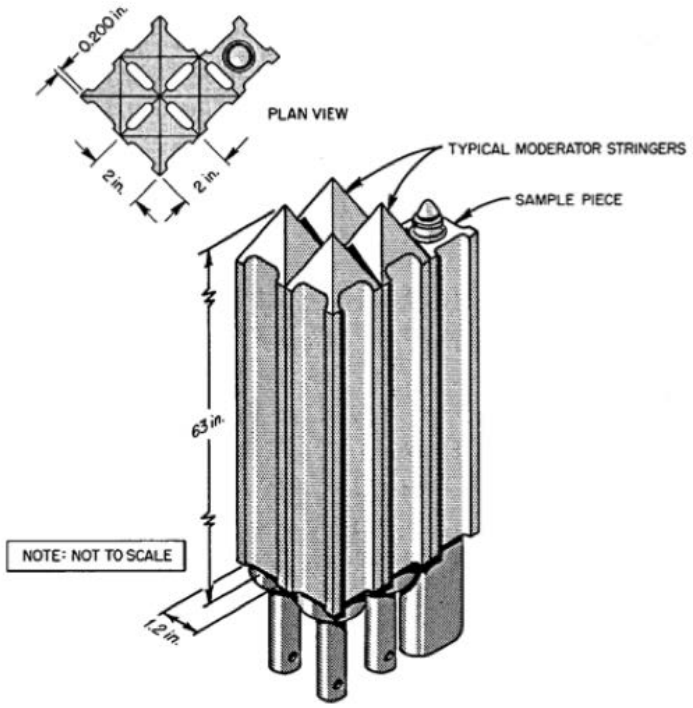


**Figure 6. Dimensions and arrangement of the MSRE graphite stringers [24].**

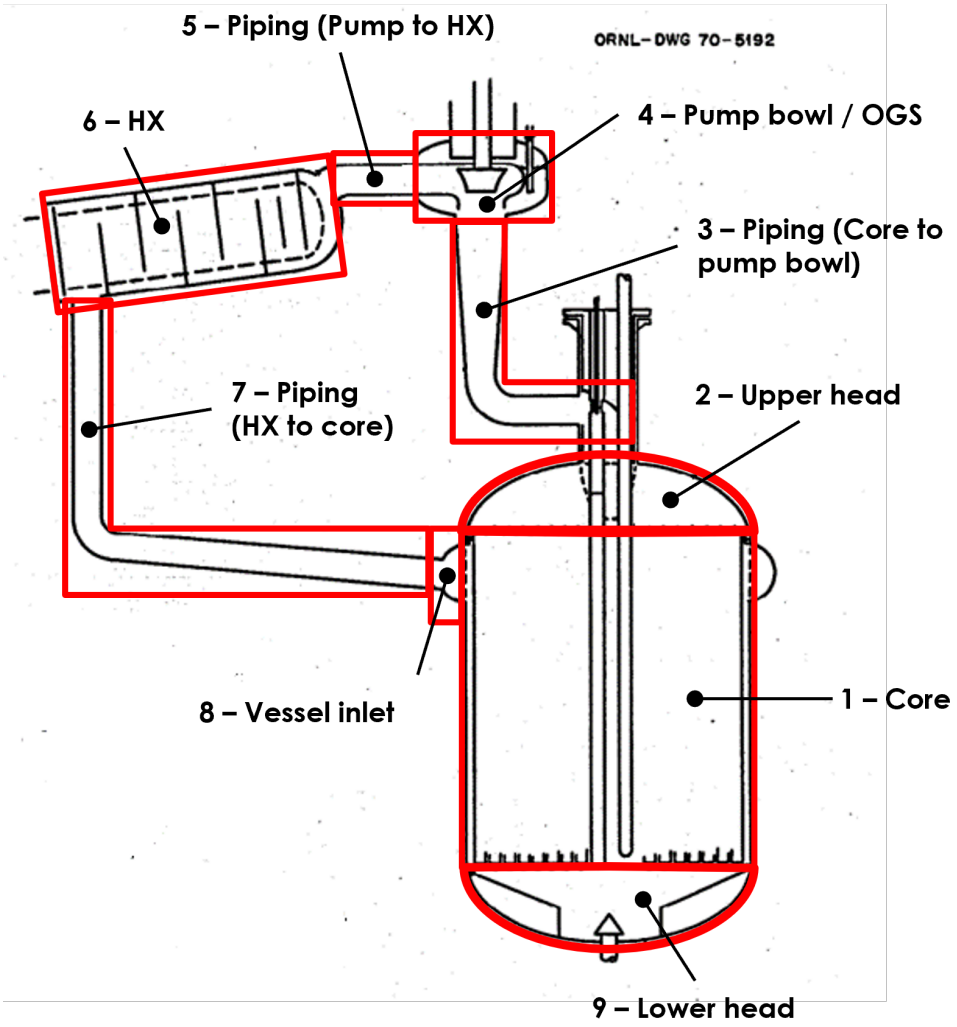


**Figure 7. Segments of the MSRE loop (modified from [25]). "OGS" indicates the off-gas system, and "HX" indicates the heat exchanger.**

## 3. SCALE MODELING APPROACH

For MSR neutronics and fuel cycle analysis, it is important to consider (1) system-level depletion with continuous feeds and removals, which occurs on a core lifetime scale (days-to-years) and determines system-average inventory, one-group cross section and transition matrix elements, and (2) the nuclide spatial distribution that considers the flow of the fuel salt through the loop, which occurs on a loop transit timescale (seconds-to-hours) and determines nuclide inventory and corresponding heat generation in the different regions throughout the loop. Given the disparity in these timescales, it is convenient to perform the analyses separately.

System-level depletion is modeled with SCALE's reactor physics sequence, TRITON. TRITON coordinates the processing of cross sections, the neutron transport calculations for 1D, 2D, and 3D configurations, and the depletion and decay to estimate the isotopic concentrations of depleted mixtures, mixture-wise power and burnup, the neutron flux, and other quantities as a function of burnup. The cross-section processing prepares multigroup or continuous-energy cross sections for the neutron transport calculation. The neutron transport calculation results in material-wise collapsed 1-group fission and removal cross sections and energy-dependent flux which are transferred together with the material compositions to the depletion solver for the depletion or decay calculation. The material compositions are then updated, and the next neutron transport calculation is run. For the cross-section processing, TRITON invokes the XSProc module; for depletion and decay, TRITON invokes Oak Ridge Isotope Generation code (ORIGEN); and for the neutron transport calculations, TRITON can be used in combination with SCALE's deterministic 1D XSDRN and 2D NEWT solvers and the 3D Monte Carlo codes KENO-VI and Shift. In this work, TRITON is used in combination with KENO-VI using continuous-energy cross sections (TRITON-KENO).

To adequately simulate the fuel salt inventory of MSRE, the removal of noble gases (mainly the fission products Xe and Kr) via the OGS and the removal of noble metals (Se, Nb, Mo, Tc, Ru, etc.) through plating out at the HX must be considered. Recent enhancements in TRITON (TRITON-MSR) [12, 13] allow these nuclide removals through the use of the new *flow* block that permits the specification of nuclide feed and removal rates for specified materials as a function of time.

To determine the spatially dependent nuclide inventory throughout the system, the depletion solver ORIGEN is used standalone. The code is widely used to compute time-dependent concentrations, activities, and radiation source terms for a large number of isotopes created or depleted concurrently by neutron transmutation, fission, and radioactive decay. ORIGEN has the unique ability (1) to simulate continuous nuclide feed and removal, which may be used to model reprocessing of liquid fuel systems, and (2) to create alpha, beta, neutron, and gamma decay emission spectra (not utilized here).

The following models were developed to determine system-level and spatially dependent nuclide inventory in the MSRE (see workflow in Figure 8):

1. TRITON-KENO model of an axially reflected slice through the core center: calculation of the burnup-dependent system-level nuclide inventory and corresponding collapsed one-group cross sections under consideration of nuclide removal through the OGS and at the HX.
2. TRITON-KENO model of the full 3D core using fuel salt inventory determined in step 1: calculation of 3D core power and flux distributions and reactivity coefficients at a single point in time (TRITON-KENO).
3. ORIGEN model of MSRE's loop using the flux distribution in the core determined in step 2 and the system-average fuel salt inventory from step 1 as a starting point: calculation of spatially dependent nuclide inventory throughout the system under consideration of nuclide removal through the OGS.

These models and the workflow are further detailed in the following sections. The system-average fuel salt inventories $\bar{N}_i$ and region-wise fuel salt inventories $N_i$, reactivity coefficients $\alpha$, total effective delayed neutron fraction $\beta_{\text{eff}}$, power distributions $P_f(r,z)$, and decay heat $P_d$ determined through the different models are provided to the MELCOR team at SNL for subsequent severe accident analyses with the MELCOR code [2].

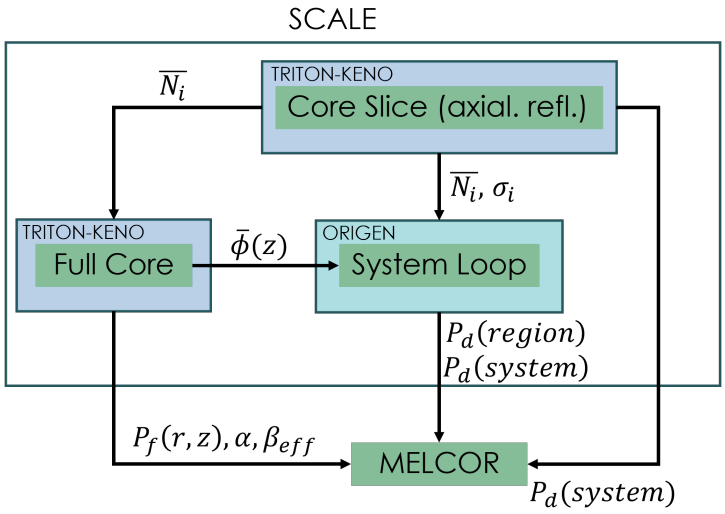


**Figure 8. MSR modeling approach with SCALE.**

### 3.1 CORE SLICE TRITON-KENO MODEL FOR TIME-DEPENDENT SYSTEM-AVERAGE NUCLIDE INVENTORY

System loop analysis requires the ability to track the spatial distribution of nuclides throughout the loop as well as the longer time evolution of the nuclides in the system. To this end, one assumes at a given depletion step (1) representative one-group nuclide transition matrix elements (explained in greater detail below) and (2) an average system-level nuclide inventory. Item (1) avoids many expensive and superfluous neutron transport calculations, as the transition matrix elements only change significantly over several days-to-months; item (2) circumvents the computational expense implied by the simultaneous spatial tracking of nuclides at the loop transit timescale.

By using a TRITON-KENO model of an axially reflected slice through the core's center (Figure 9), *representative* system-average nuclide inventories and transition matrix elements are determined at certain points in time (time frame of days-to-years) while reducing the computational burden as compared to a full core calculation. Although only a slice is simulated, the system-average nuclide inventory (i.e., the inventory in the core and the loop) is approximated by adjusting the specific power to consider the residence time of the fuel outside the core. Furthermore, by application of TRITON with flow definitions, nuclide removal in the OGS and at the HX (both outside of the core) can be considered.

Nuclide removal is requested by specification of material-dependent removal constants in the corresponding TRITON input block. In order to understand the use of these removal constants, the first order ordinary differential equation (ODE) can be interrogated—the equation that ORIGEN solves to determine the concentration of nuclides at specific points in time through consideration of nuclide production from fission or decay or through a source, and nuclide loss due to decay, irradiation or other means.

The time-dependent 0-dimensional concentration of a nuclide in the fuel loop is given by

$$\frac{dN_i}{dt} = \sum_{j\neq i}^{M} \left(l_{ij}\lambda_j + f_{ij}\sigma_i\phi\right) N_j(t) - \left(\lambda_i + \sum_{l}^{W} \lambda_{i,l,rem} + \sigma_i\phi\right) N_i(t) + S_i(t), \tag{1}$$

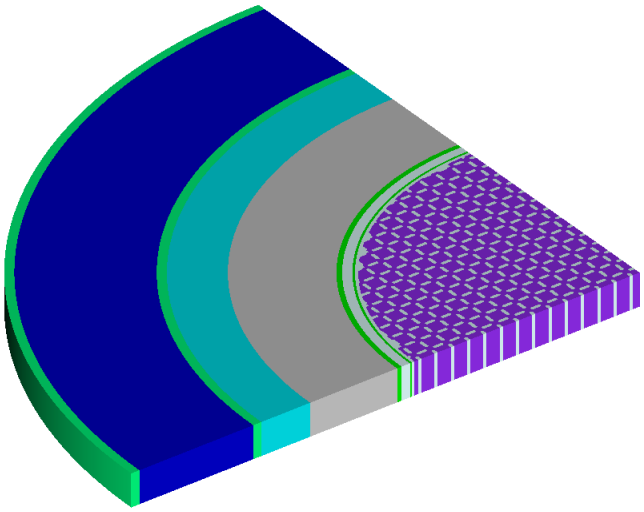

**Figure 9. TRITON-KENO model of an axially reflected slice through the core center (quarter of the model).**

where

$N_i$ is the amount of nuclide $i$ of the $M$ nuclides considered (atoms),

$\lambda_i$ is the decay constant of nuclide $i$ ($s^{-1}$),

$l_{ij}$ is the fractional yield of nuclide $i$ from decay of nuclide $j$,

$\sigma_i$ is the spectrum-averaged removal cross section for nuclide $i$ (barn [$10^{-24}$ $cm^2$]),

$f_{ij}$ is the fractional yield of nuclide $i$ from neutron-induced removal of nuclide $j$,

$\phi$ is the angle- and energy-integrated, time-dependent neutron flux (neutrons $cm^{-2}$ $s^{-1}$),

$\lambda_{i,l,rem}$ is the removal constant defining continuous removal of nuclide $i$ to waste stream $l$ of the $W$ waste streams considered ($s^{-1}$), and

$S_i$ is the time-dependent source term (atoms $s^{-1}$)

As a point of emphasis, $\lambda_{i,l,rem}$ is a physically fictitious, user-defined value which represents the rate of removal of a particular nuclide *from a material*, as in the removal of specific nuclides through off-gassing, plating out, fuel processing, and so on. Given the many transport phenomena that can be accounted for by this constant, it is common in ORNL MSR literature to express a nuclide's (or group of nuclides) total removal constant by a characteristic cycle time. This cycle time quantifies the amount of time it takes to *fully* remove a chemical species from the fuel salt [16]. In general, the relation between $\lambda_{i,l,rem}$ and the cycle time is given by [13]:

$$\lambda_{i,l,rem} = \frac{|\ln(1-r)|}{\Delta t}, \tag{2}$$

where $r$ is the unit-less removal fraction, and $\Delta t$ is the cycle time (s). The shortfall of this definition is noted: when a nuclide is considered *fully* removed, then $r \to 1$, $\lambda_{i,l,rem} \to \infty$, and (2) become invalid. To avoid this issue, some value $r < 1$ must be used, such as $r = 0.999$, to approximate a nuclide's full removal. More physically representative models have been developed to quantify removal rates for MSRE—particularly for

noble gases and noble metals—for which methods and results can be found elsewhere [26, 27]. Appropriate removal rate constants from these studies are used here.

Equation (1) sufficiently describes the approximate time-dependent nuclide concentration and may be represented in the following matrix form:

$$\frac{d\overline{N}}{dt} = \overline{\overline{A}}\,\overline{N} + \overline{S}, \tag{3}$$

where $\overline{\overline{A}}$ is commonly referred to as the "transition matrix" with size $M$ by $M$ (for $M$ nuclides considered). The elements $\overline{\overline{A}}$ are, correspondingly:

$$a_{ij} = \begin{cases} l_{ij}\lambda_j + f_{ij}\sigma_i\phi & i \neq j \\ -\lambda_i - \sum_l^W \lambda_{i,l,rem} - \sigma_i\phi & \text{else.} \end{cases} \tag{4}$$

Given the relatively small number of potential paths decaying or transmuting nuclide $j$ into nuclide $i$, the transition matrix is sparse, consisting of roughly 1% non-zero elements. In the TRITON calculation, values $f_{ij}$, $l_{ij}$, $\sigma_i$, and $\phi$ are determined through the transport calculation for the depletable materials. For brevity, it is often only referred to as one-group cross sections or transition matrix elements, although all of these values are intended. ORIGEN then uses these to solve the first-order ODE (3) to yield time-dependent, system-level equilibrium nuclide inventory, $\overline{N}$, where

$$\overline{N} \equiv \begin{bmatrix} N_i \\ \vdots \\ N_M \end{bmatrix}. \tag{5}$$

### 3.2 FULL CORE TRITON-KENO MODEL FOR POWER AND FLUX DISTRIBUTIONS AND REACTIVITY COEFFICIENTS

To determine the spatial distribution of the neutron flux and the power in the core, a TRITON-KENO 3D core model was developed. As mentioned above, a model developed based on the MSRE IRPhEP benchmark [19] was used as basis for the model in this work. While TRITON supports the calculation of the neutron flux and the fission rate in a user-defined mesh superimposed over any geometry, the calculation of the power profile requires discretization of the model into individual regions with individual mixtures to obtain mixture-dependent power levels. In a first step, the distribution of the neutron flux and the fission rate was investigated using simple mesh tallies. Based on the observed profiles, the core model was discretized into 35 axial zones and 8 radial zones (Figure 10). The major core region was finely discretized into 30 axial regions, and the salt was homogenized in the lower head and the upper head (and therefore throughout the out-of-core loop).

The specific power of the individual mixtures from the TRITON-KENO calculation of the discretized model corresponds to zone-wise specific power levels in the core. These data are post-processed to obtain normalized axial and radial power profiles that yield a total power of 1. The obtained power follows the following convention: with the radial power profiles $p(z, r)$ in each zone normalized to 1, and the radially-integrated axial power profiles $f(z)$ also normalized to 1, the power in each zone is given as:

$$P_f(z, r) = c \cdot f(z) \cdot p(z, r), \tag{6}$$

where $c$ is a scaling factor that allows the total power to be scaled up or down to the desired level.

A similar calculation can be performed for the neutron flux profile. In particular, the radially-integrated integrated neutron flux profile $\overline{\phi}(z)$ can be calculated from mixture-specific fluxes. This flux profile is used in the calculation of location-dependent nuclide inventory as detailed in Section 3.3.

The TRITON-KENO full core model is also used to calculate temperature-dependent reactivity feedback. Reactivity coefficients were determined for temperature changes in the graphite structure and for temperature and simultaneous density changes in the fuel salt. The effective delayed neutron fraction $\beta_{\text{eff}}$ and the xenon worth were also determined.

### 3.3 ORIGEN MODEL FOR LOCATION-DEPENDENT NUCLIDE INVENTORY

Although the depletion of the axial core slice model was used to determine time-dependent system-average nuclide inventory on a time scale on the order of days-to-years, it is of interest to determine the inventory in each region of the loop. For example, if there were a leak at a specific location in the loop, then an improved approximation of the inventory at this location could be provided instead of providing the system-average inventory. Likewise, it is interesting to understand whether the inventory changes significantly between the different regions, i.e. whether assuming system-average inventory is sufficient for a good approximation of inventory and decay heat. Differences in individual nuclide concentrations (especially short-lived nuclides) can be expected, but it should be noted that MELCOR is only considering a few element classes in which the isotopes for multiple elements are lumped together.

In theory, a TRITON-KENO model can be developed to determine location-dependent inventory, but ORIGEN was used here in a *slug flow* modeling approach. A slug of fuel salt was followed through the different regions on the loop as it experienced varying flux levels for varying residence times. As indicated in Figure 7, 9 regions were distinguished in this model: lower reactor vessel head, core, upper reactor vessel head, pump bowl/OGS, HX, vessel inlet, and the individual piping that connects the individual loop elements. The core was further sub-divided into 30 axial zones in order to be able to consider the axial flux profile in the core. Although possible, no radial zones were considered for the core.

The residence time of the fuel slug in the individual regions was a result of the volumes, as listed in Table 2. The integrated axial flux profiles $\overline{\phi}(z)$ from the 3D TRITON-KENO calculation was applied to the different regions in the core. It was assumed that all regions outside the core did not to experience neutron flux; these regions were considered as regions with only nuclide decay. ORIGEN's nuclide removal capability was used to remove noble gases in the region of the OGS. Instead of a removal constant as specified in the TRITON model, ORIGEN requires the specification of the *fraction* of *retained* nuclides.

A chain of ORIGEN inputs was developed, with each ORIGEN input corresponding to a fuel slug traveling one time through the loop. The starting point for the first loop was the system-average fuel salt composition and the corresponding one-group cross sections from the TRITON-KENO slice model at 375 days. After the first loop, each following loop started with a fuel slug containing the nuclide composition of the corresponding previous loop. For individual regions, the concentrations of various nuclides with different half lives was investigated as a function of the number of loops to observe the convergence of these concentrations within the region. For a specific loop, the concentrations of nuclides in a slug were then investigated while traveling through the loop (i.e. the nuclide concentration was determined as a function of the regions) to study their variance over the loop. Because the loop transit time of MSRE was only 25.2 seconds and only a few transits were calculated with ORIGEN, the final location-dependent inventory still approximately corresponds to the operation time of 375 days (only a few minutes after).

Nuclide concentrations at various axial locations in the core were obtained with this approach. These concentrations were used in a sensitivity study to update the TRITON-KENO full core model to observe the impact of the use of system-average nuclide densities vs. spatially dependent nuclide densities on the power and flux profile.

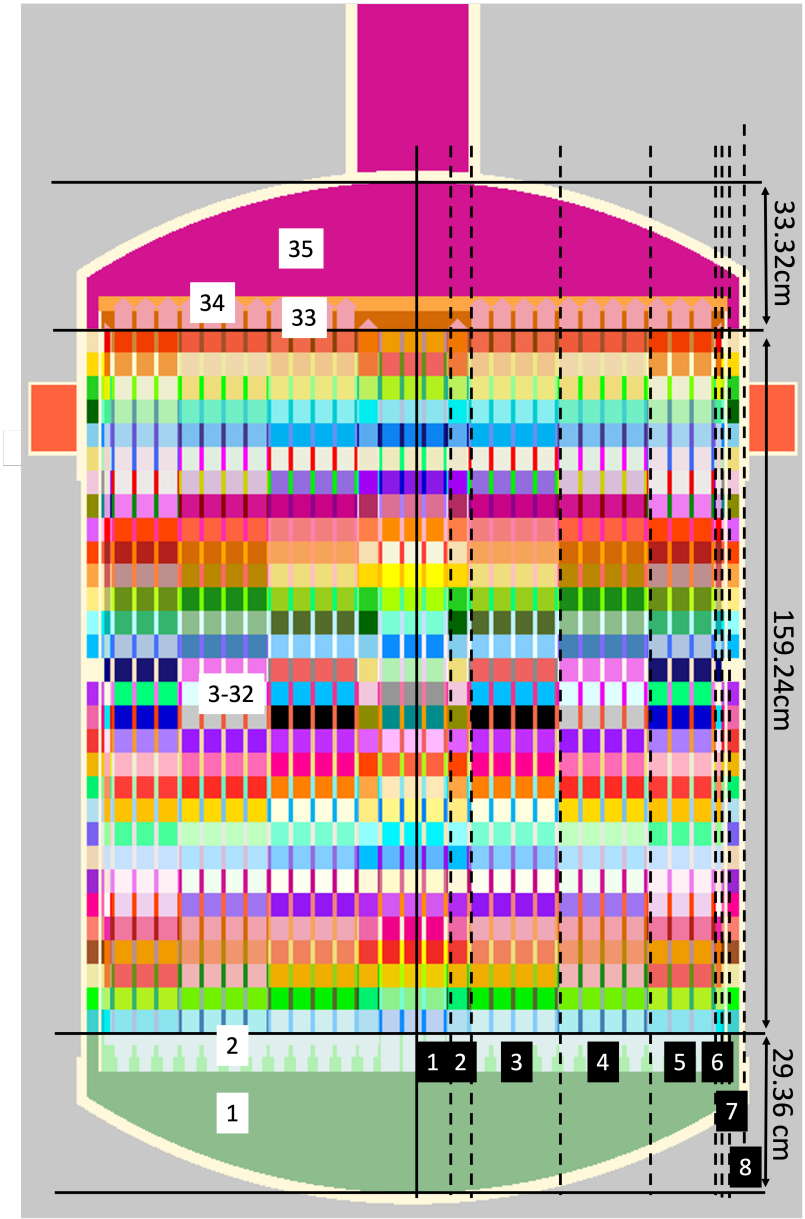


**Figure 10. Discretized 3D full core SCALE model.** Axial zones are indicated in white boxes, and radial zones in black boxes.

## 4. ANALYSIS OF THE TIME-DEPENDENT SYSTEM-AVERAGE NUCLIDE INVENTORY

When using an axially reflected core slice model as described in Section 3.1 to generate nuclide inventories over longer time periods, the fuel salt throughout the system is modeled with a representative neutron flux spectrum. Heuristically, this is a reasonable approximation: given a loop transit time of 25.2 seconds (i.e., more 3,400 transits per day), long-term nuclide inventory trends are dominated by averaged reactor physics quantities.

To justify the use of an representative spatially independent neutron flux (and corresponding one-group cross sections), Figure 11 compared the neutron flux in the fuel salt of the slice model to the neutron flux in the full core model at various radial positions in the axial middle of the core. The flux in the slice model agrees well with the flux of the full core model in the main radial region outside the center where the flux shows changes caused by the control rod channels and sample basket.

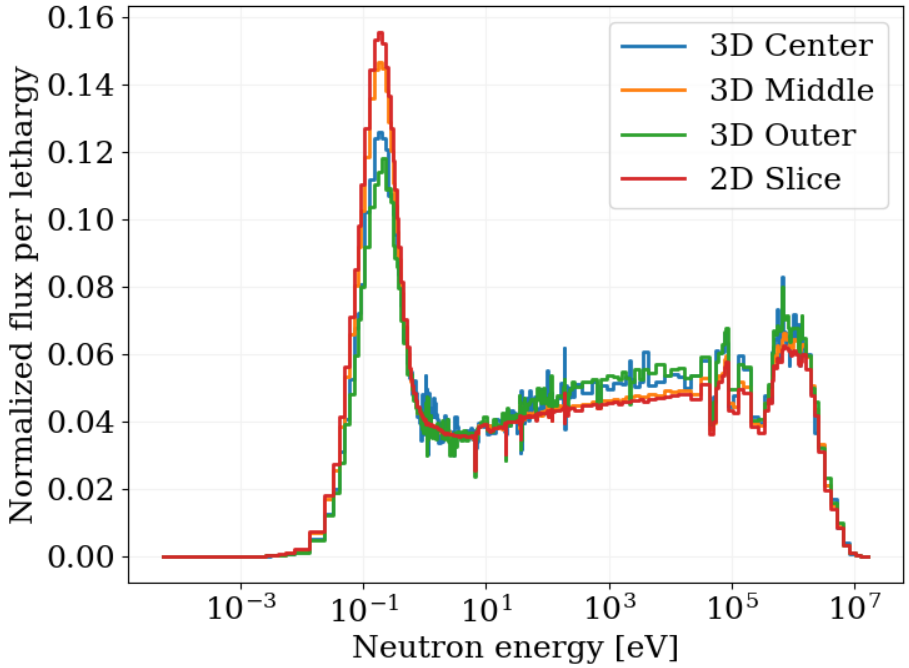


**Figure 11. Comparison of the normalized neutron flux in the slice model to the full core (center, middle, and outer region in the core center).**

Considering that the fuel spends 68% of its time within the reactor vessel and the remaining time in the loop, the specific power is determined by dividing the total core power of 8 MWth by the system's (i.e., core+loop) initial heavy metal mass of 0.218 metric ton initial heavy metal (MTIHM). This results in the specific power of 36.69 MW/MTIHM applied for the depletion calculation. Although the *in-core* power density is much greater, this ensures that the approximate time the fuel spends in $\phi = 0$ regions outside out core is taken into account.

The slice is depleted in 7 steps to 375 days; this relatively coarse time grid is sufficient to obtain adequate estimates of fuel inventory. Each neutron transport calculation was converged to reach a statistical uncertainty of the eigenvalue of 20 pcm. The whole depletion calculation took approximately 8,900 CPU-hours.

## 4.1 REMOVAL RATE DETERMINATION

Removal of nuclides from the fuel salt during operation is a key difference in the calculation of MSR fuel inventory compared to that of a solid-fueled reactor. The correct determination of the removal constants $\lambda_{i,l,rem}$ for TRITON's new flow block is essential for ensuring the correct representation of nuclide removal and therefore the nuclide inventory, the neutron flux, and the one-group cross sections.

Removal rates for the MSRE were derived from MSRE's experimental data. Two removal paths are considered: (1) noble gases being actively pumped out of the system via the OGS, and (2) noble metals being deposited (i.e., *plated-out*) on surfaces within the loop. Figure 12 illustrates the removal rates applied in this study, and the subsequent subsections discuss the method to obtain these removal constants. For simplicity, Figure 12 does not show the holdup tank and filter in the OGS. TRITON tracks the removed nuclides in separate materials in which nuclide decay is simulated (but without irradiation, i.e., zero flux).

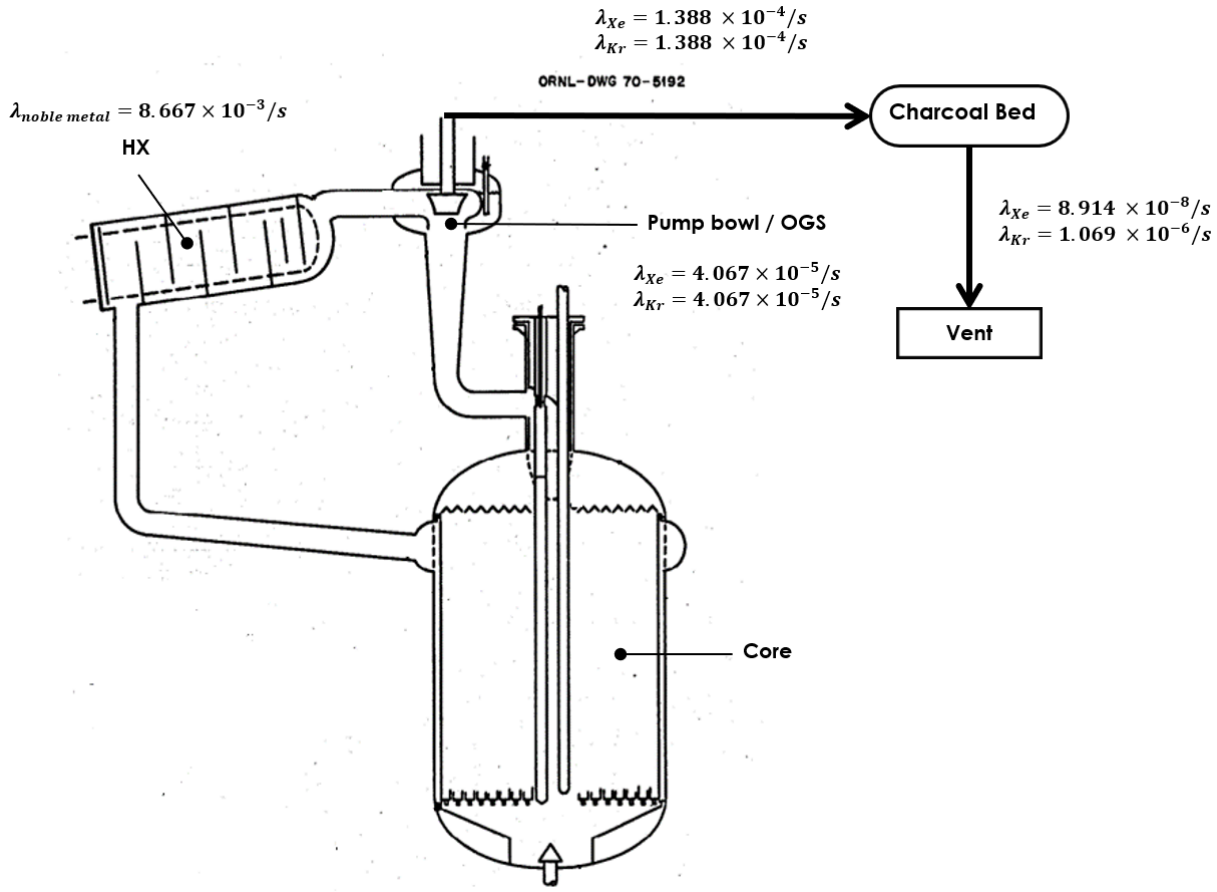


**Figure 12. Removal rate used in the axial core model.**

### 4.1.1 REMOVAL OF GASEOUS FISSION PRODUCTS

Gaseous fission products such as xenon (Xe) and krypton (Kr), are actively removed from the fuel salt via the OGS [24]. From a reactor physics standpoint, major concerns are (1) the adequate estimation of the Xe inventory in the fuel salt resulting from the significant neutron absorption in $^{135}$Xe and (2) the impact on the reactor's reactivity. Although more in-depth experimental work was performed to monitor krypton [26] in the OGS, the main experimental basis for this study is the quantification of Xe via the Xe poison fraction (PF), as

defined by

$$PF = \frac{\Sigma_a \left(^{135}\mathrm{Xe}\right)}{\Sigma_a \left(^{235}\mathrm{U}\right)}. \tag{7}$$

For MSRE, the PF is reported to have varied between 0.3% and 0.4% [26]. To at least establish a quasi-physical model as a starting point, an approach used by Valdez et al. [16] is replicated. (A more physical basis for modeling the OGS mass transport can be found elsewhere [26]). In Valdez et al. [16], the removal rate, $\lambda_{i,l,rem}$, is represented as a function of a removal efficiency $\eta$ and the ratio of the salt flow rate $\dot{V}$ ($m^3$/s) through the gas-liquid separator loop and the total volume of salt in the primary fuel loop $V$:

$$\lambda_{i,l,rem} = \frac{\dot{V}}{V}\eta. \tag{8}$$

Assuming $V = 1.996$ $m^3$, $\dot{V} = 0.003153$ $m^3$/s [24], and $\eta = 0.15$ [26], a removal fraction of $\lambda_{i,l,rem} = 2.370 \times 10^{-4}$ 1/s is found. However, this removal rate yields a lower PF value compared to the measurement. Therefore, the removal rate was gradually reduced until a more representative PF of 0.4% was obtained. This was achieved through an efficiency of $\eta = 0.026$, corresponding to a removal rate of $\lambda_{i,l,rem} = 4.067 \times 10^{-5}$ 1/s. This removal rate was used in the final TRITON model for the removal rate of Xe and Kr from the fuel salt into the OGS.

The removal rate from the OGS to the charcoal bed was derived by considering the hold-up time at the piping, which is reported to be about 1.5 hours to allow the short-lived fission products to decay to further decrease the heat generated in the charcoal bed. Similarly, the removal rate from the charcoal bed to the vent is considering the hold-up time to allow the gaseous fission products to decay to stable elements. It is reported that Xe and Kr are held for 90 and 7.5 days in the charcoal bed, respectively [24].

The impact of removing Xe and Kr in the OGS on the system-average Xe and Kr densities in the fuel salt is visible in Figure 13. In a regular depletion calculation without removal, the Xe and Kr densities increase over time because of the build-up of fission and decay products; the removal of Xe and Kr in the OGS causes lower densities that become constant after a few days. The impact of the Xe removal on reactivity is significant: because the removal of Xe results in less neutron absorption from $^{135}$Xe, the eigenvalue $k$ of the slice is between 750 and 930 pcm higher compared to a system without Xe removal. Table 3 shows the removed amounts of Xe and Kr at the end of the depletion calculation: approximately 30.6 liters.

Because the OGS is tracked as an individual mixture in TRITON, the densities in the OGS and the system (fuel salt in core+loop) can be inspected individually (Figure 14). Besides the constant densities in the fuel salt, the densities in the OGS are also constant because Xe and Kr are constantly removed from the OGS to a charcoal bed (see Figure 12).

**Table 3. Calculated amount of removed noble gases and noble metals at 375 days**

| Element group | Amount removed at 375 days |
|---|---|
| Noble gas (Xe + Kr) | 0.170 kg / 30.6 L |
| Insoluble metals (Mo + Tc + Ru + Rh + Pd + Ag + Sb) | 0.611 kg |
| Sometimes soluble metals (Se + Nb + Te) | 0.057 kg |

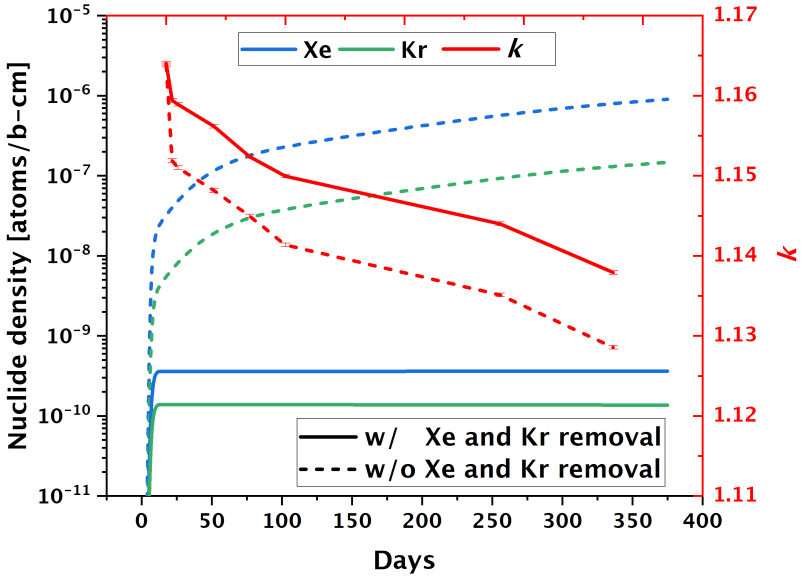


**Figure 13. Densities of Xe and Kr in the fuel and system eigenvalue $k$ with and without consideration of Xe and Kr removal in the OGS.**

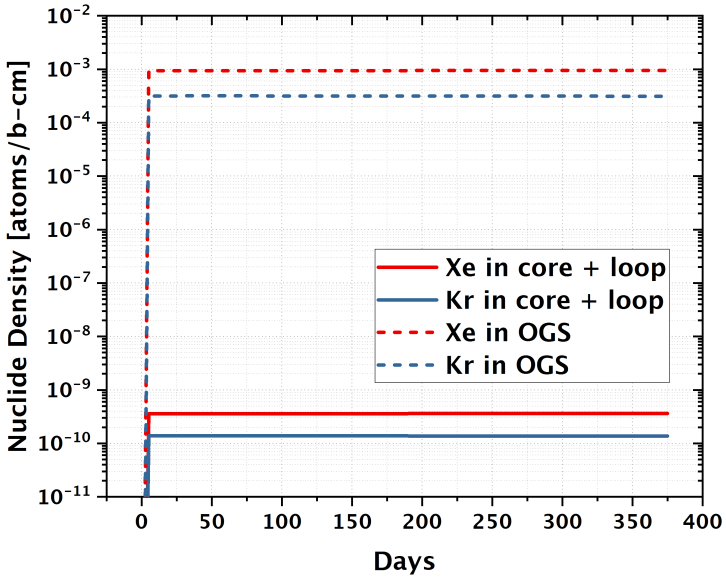


**Figure 14. Densities of Xe and Kr in the fuel salt (core+loop) and the OGS.**

### 4.1.2 PLATE-OUT OF NOBLE METAL FISSION PRODUCTS

Noble metal fission products—specifically Nb, Mo, Ru, Sb, and Te for MSRE—are reduced by $UF_3$ in the fuel salt and are thus in the metallic state. They migrate to various surfaces inside the whole system (e.g., HX, OGS, pipes) and adhere to them. The MSRE's relative distribution of the noble metals after operation was reported by Kedl [27] and is summarized in Table 4. Thus, 99% of the noble metal fission products reside outside the core, and some of them decay later to the halogens I and Br. To demonstrate TRITON's capability to consider the effect of plate-out, the noble metals' adhesion to surfaces was considered in the form of noble metal removal from the fuel salt into a separate mixture. This mixture could be corresponding to plated out material at a specific location in the loop, such as the HX. Although it would be possible to consider separate materials for individual locations, the slice depletion here simplified the effect as a removal into just one material.

**Table 4. Noble metal distribution in MSRE when operated with $^{235}$U [27]**

| | Fraction (%) |
|---|---|
| HX | 40 |
| Hastalloy-N surfaces in loop | 50 |
| Graphite surfaces in-core | 1 |
| Pump bowl, overflow tank, OGS, etc. | 9 |

The removal rate $\lambda_{i,l,rem}$ for a nuclide $i$ to waste stream $l$ (see Eq. 1) is calculated via:

$$\lambda_{i,l,rem} = \frac{1}{V} \cdot h_{i,l} A_l, \tag{9}$$

where $h_{i,l}$ is the mass transfer rate (m/s) of nuclide $i$ to waste stream $l$, $A_l$ is the surface area of waste stream $l$, and $V$ is the total system fuel salt volume (see Table 2). Table 5 provides the mass transfer rate and surface area values for individual components in the loop from Kedl [27], together with the corresponding calculated removal rates. The total removal rate was used to simulate the plate-out in the depletion calculation.

Of note is the large mass transfer coefficient attributed to the transfer of noble metals into the bubbles in the fuel salt that are created through the addition of helium by the pump bowl bubblers, pump bowl purge and overflow tank bubblers. The fraction of bubbles in the MSRE's fuel salt during the operation with $^{235}$U was 0.02-0.045%, with average bubble sizes of approximately 0.012 cm [27]. It is explicitly noted that the bubbles are not modeled in any of the developed SCALE models used in this work (i.e., the salt density assigned reflects that of a *bubble-less* liquid).

The TRITON model considered the plate-out of Se, Nb, Mo, Tc, Ru, Rh, Pd, Ag, Sb, and Te. The resulting buildup of noble metals in the HX is depicted in Figure 15. The total masses of the removed noble metals are shown in Table 3.

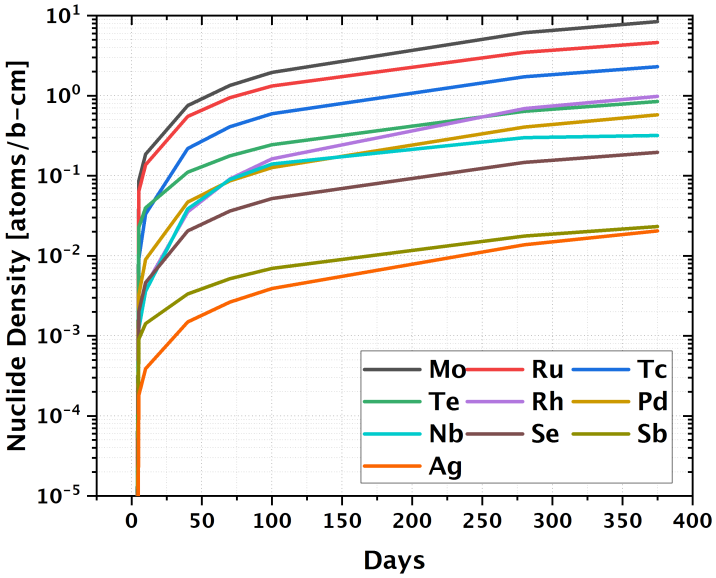


**Figure 15. Densities of noble metals plated out.**

**Table 5. Noble metal mass transfer rate, surface area, and resulting removal rate**

| Component | $h_{i,l}$ ($10^{-6}$ m/s) [27] | $A_l$ ($m^2$) [27] | $\lambda_{i,l,rem}$($10^{-4}$ $s^{-1}$) |
|---|---|---|---|
| HX | 46.57 | 29.26 | 6.827 |
| Fuel loop piping, core and pump volute | 104.1 | 6.60 | 3.441 |
| Core wall cooling annulus | 43.18 | 14.31 | 3.095 |
| Core graphite (exposed to salt) | 5.334 | 136.10 | 3.637 |
| Miscellaneous (pump impeller, core support grid, etc.)[a] | – | – | 1.695 |
| Bubbles | 423.3 | 32.05 | 67.978 |
| Total | – | – | 86.674 |

[a] Set in [27] as 10% of the above 4 components

### 4.2 INVENTORY AND DECAY HEAT AT 375 DAYS

Figure 16 depicts the masses of the relevant nuclides in the fuel salt calculated with TRITON. In addition to $^{234}$U, $^{235}$U, and $^{238}$U, the presented nuclides correspond to the top contributors to the decay heat after shutdown. Since the reactor was operating at a low power of only 8 MWth at a flux level of approximately $1.88 \times 10^{13}$ n/cm$^2$-s, the burnup after 375 days was small with 13.76 GWd/MTIHM and the $^{235}$U and and $^{238}$U consumption rates were low with 5.627% and 0.455%, respectively. As a result, only small amounts of fission products were produced and only little $^{239}$Pu was build-up (less than 0.5 kg).

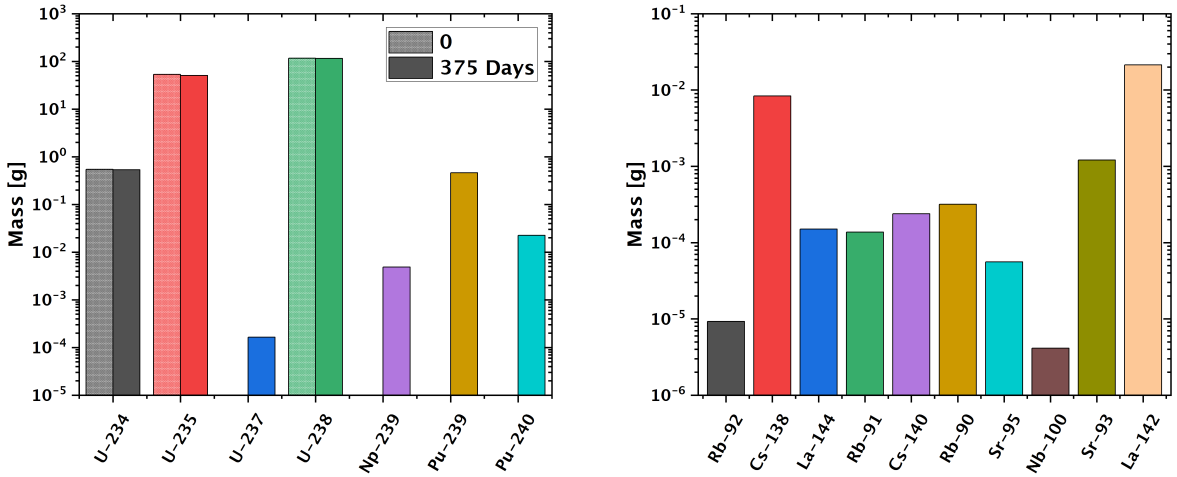


**Figure 16. Mass of actinides (left) and fission products (right) at 375 days**

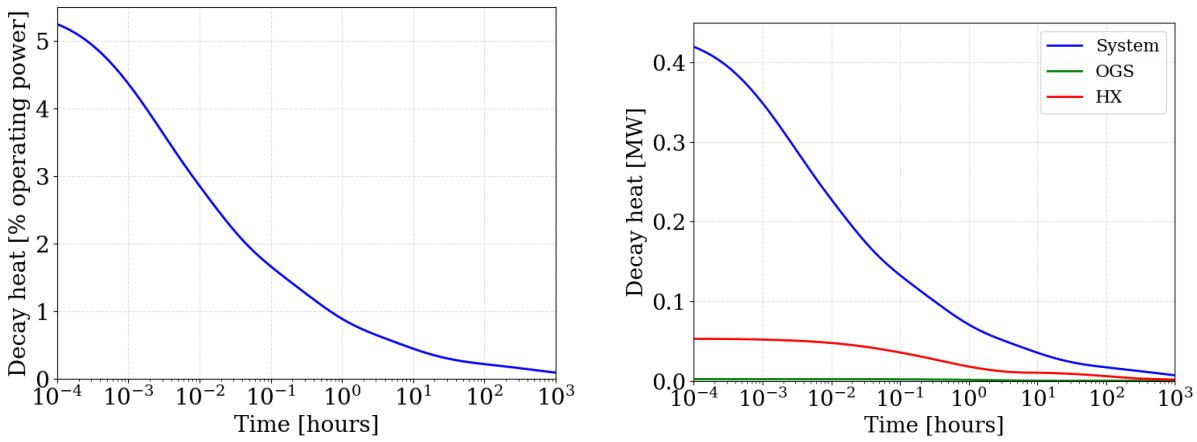


**(a) Relative decay heat of the fuel salt in the system expressed in relation to the operating power**

**(b) Absolute decay heat of the fuel salt in the system, the OGS, and from plated-out noble metals (HX)**

**Figure 17. Decay heat after shutdown at 375 days.**

Figure 17a shows the decay heat of the fuel salt in the system (core+loop) after shutdown at 375 days. The decay heat is slightly above 5% of the operating power of 8 MWth, or slightly above 0.4 MW. The decay heat of a typical LWR at the end of a cycle is usually on the order of 6% operating power. The decay heat is slightly less for the MSRE because of the lower burnup. Furthermore, a non-negligible amount of decay heat is generated from the plated out material (0.05 MW), which is considered separately (Figure 17b).

Figure 18 shows the top contributors to the decay heat in the fuel salt, the OGS, and from the plated out noble metals (top contributors over the entire displayed time range). For the fuel salt, the same contributors are found that are commonly found for $^{235}$U-enriched systems. For the OGS, the main contributions to the decay heat come from removed Xe and Kr isotopes and their decay products. Similarly, the top contributors for the plated out material are the noble metals and their decay products.

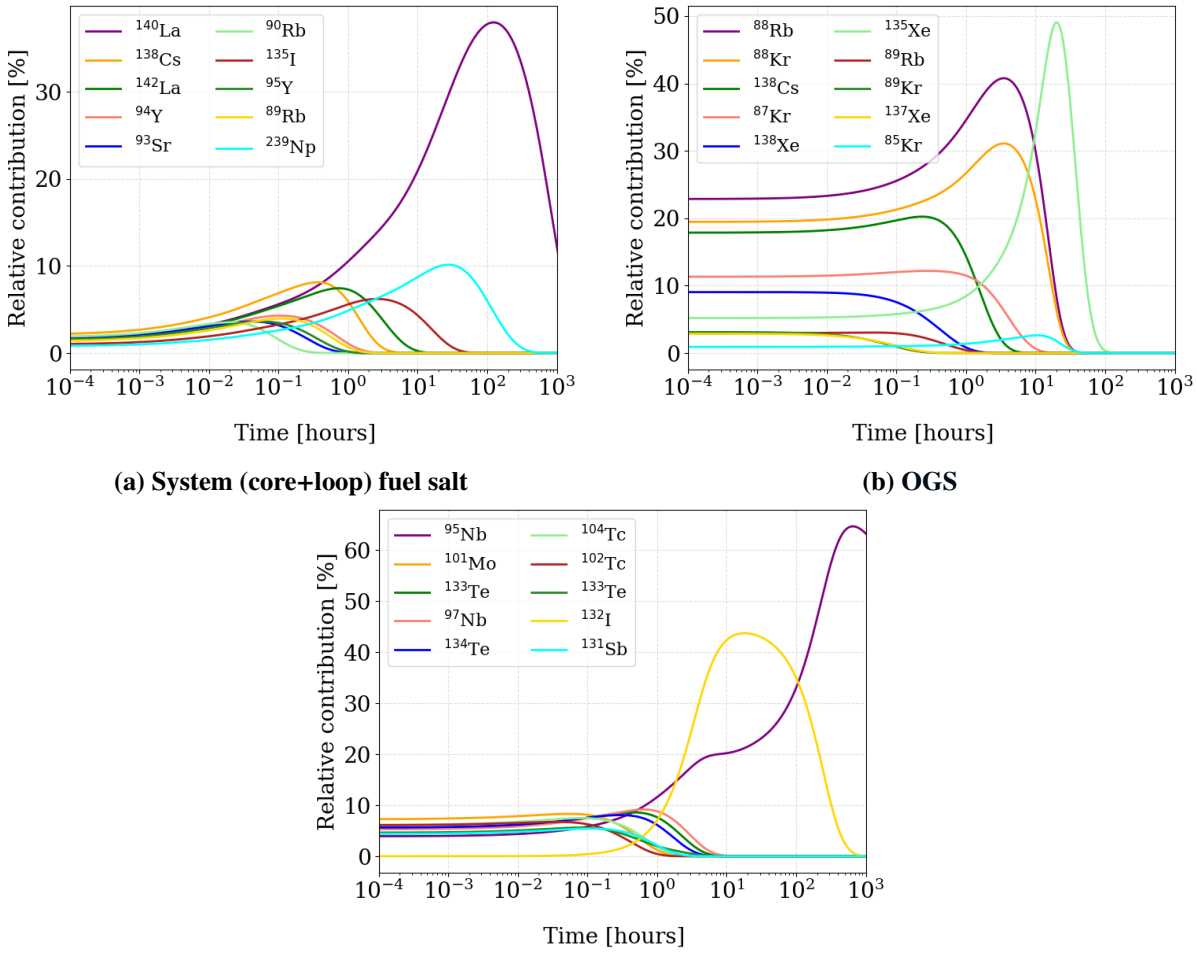


**(a) System (core+loop) fuel salt**

**(b) OGS**

**(c) Plated-out material (HX)**

**Figure 18. Top decay heat contributors to the total decay heat in individual components.** (Relative contribution of decay heat contributed by a specific nuclide to the total decay heat observed in the individual component.)

## 5. FULL CORE POWER, FLUX, AND REACTIVITY COEFFICIENT ANALYSIS

The TRITON-KENO full core calculations as described in Section 3.2 were performed for fresh fuel and also by using the fuel salt compositions generated by the axial core slice model at 375 days (Section 4). Several neutronics characteristics, including the axial and radial flux and power distributions, the total effective delayed neutron fraction $\beta_{\text{eff}}$, and the temperature reactivity coefficients for fuel salt $\alpha_{salt}$ and graphite moderator $\alpha_{graphite}$, were studied.

### 5.1 FLUX AND FISSION RATE DISTRIBUTIONS OF THE FRESH CORE

To inform the discretization for the power profile analysis, the flux and fission rate distributions of the MSRE with fresh fuel were investigated. The mesh capability in TRITON-KENO was applied to obtain spatial distributions and energy-dependent flux in different regions of the core. The resulting flux is the flux per fission neutron divided by the mesh voxel volume.

Figure 19 shows the energy-dependent neutron flux at various axial locations in the core. The thermal peak clearly shows that the MSRE is a graphite-moderated system because the thermal peak is larger than in typical LWRs. The thermal peak in the uppermost location shown is reduced because of the absorption through the control rods, which are only inserted into the top of the core.

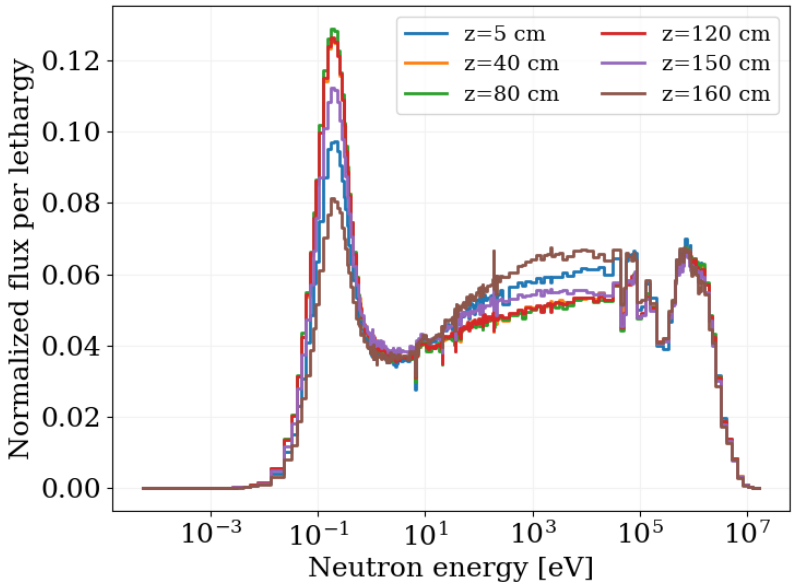


**Figure 19. Normalized neutron flux in the fresh full core at various axial locations.**

Figure 20a shows the fast (E>0.625 eV), thermal (E<0.625 eV), and total flux as a function of the radial position (in the axial center of the core); the yellow lines indicate the outer boundary of the reactor vessel. Figure 20b shows the flux in the axial location (in the radial center of the core); the yellow lines indicate the lower and upper ends of the graphite structure, and at 200 cm the upper end of the vessel (the outlet channel above the upper end of the vessel is also part of the full core model).

The slight flux depression in the radial center of the core is caused by the air-filled control rod channels and the sample basket. The axial flux distribution shows the expected sine shape with some flux in the upper

and lower plenum outside the graphite structure. The uppermost 40 cm indicate the outlet channel above the reactor vessel, in which there is only little flux. Figures 20c and 20d show the ratio between the fast and thermal flux. This is especially useful to understand spectral differences in the various regions of the core. Besides the small variation in the area of the control rod channels, the radial and axial ratios between fast and thermal flux are approximately constant over most of the core, particularly in the area of the graphite structure.

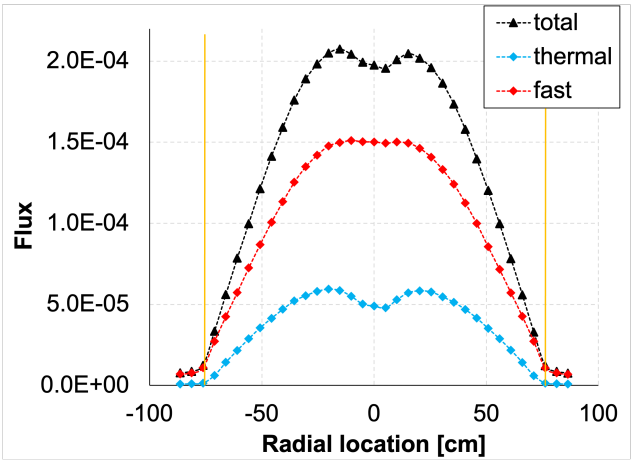


(a) Radial flux

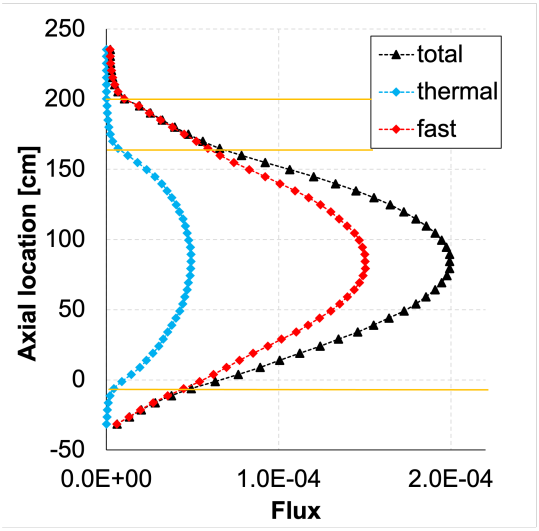


(b) Axial flux

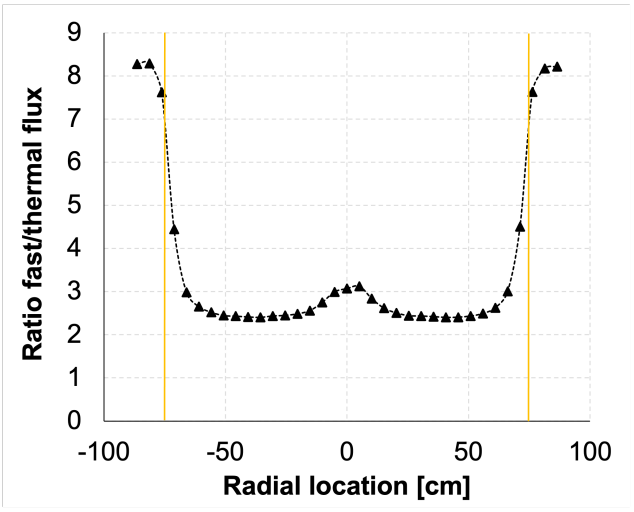


(c) Ratio of fast to thermal flux in radial direction

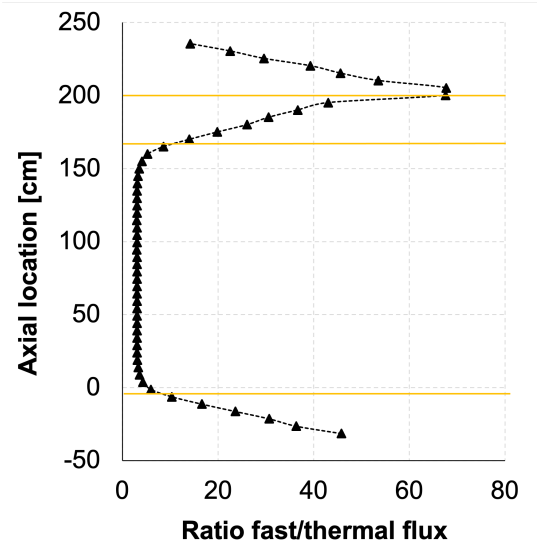


(d) Ratio of fast to thermal flux in axial direction

**Figure 20. Normalized radial and axial flux of the fresh full core**

The fission rate is approximately proportional to the reactor power, providing a useful way to obtain an initial understanding of relevant regions in the core in terms of power. Figure 21 shows color plots of the fission rate. As for the flux, the radial center of the core shows a reduction in the fission rate resulting from the empty control rod channels. In contrast, the largest fission rate was observed in the area of the sample basket where the fuel salt is flowing through a channel with less graphite. This is a first indicator that the core is over-moderated to the point that a reduction in moderator material is causing an increase in fission.

This effect can also be observed in the regions directly below and above the graphite structure where local increases in the fission rate can be observed. In particular, this analysis informed the discretization of the full core for the purpose of the power analysis by suggesting additional axial zones in these regions of slightly increased fission.

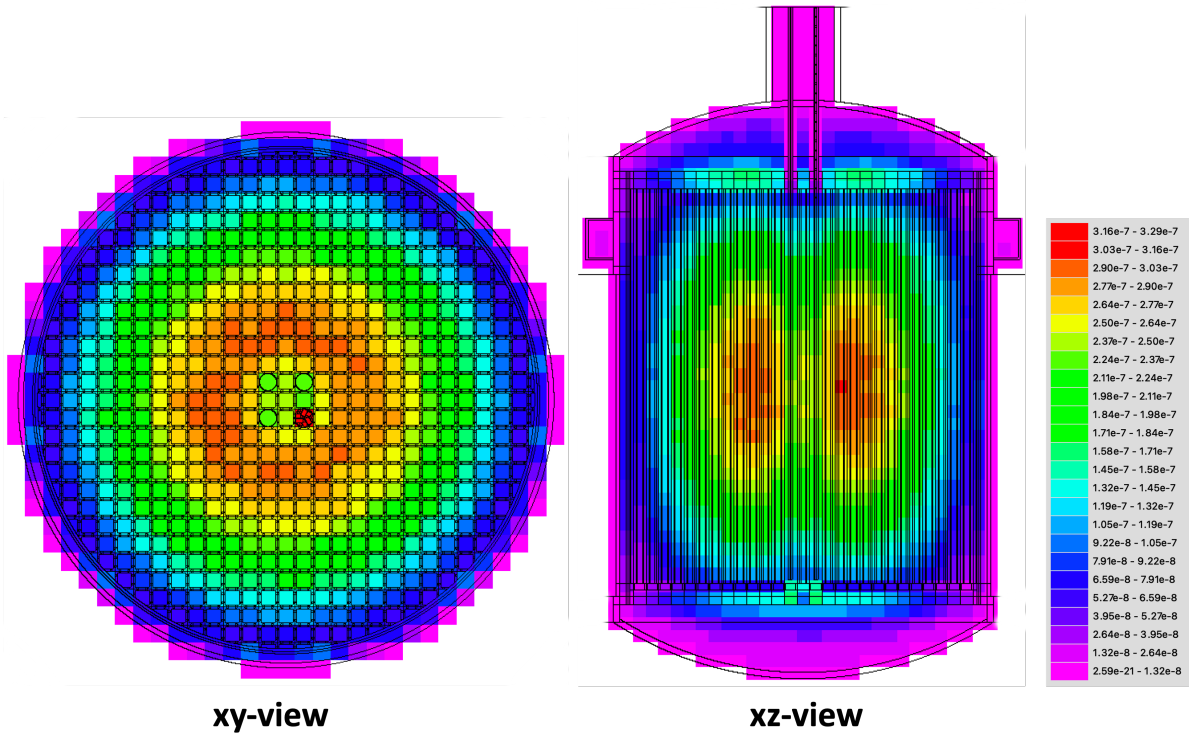


**Figure 21. Normalized radial and axial fission rates of the fresh full core.**

## 5.2 POWER PROFILES

Figure 22 shows normalized radial and axial power profiles according to Eq. (6) for various axial and radial zones, respectively. The results were obtained from a discretized core model that includes the inventory at 375 days from the slice depletion calculation. The same conclusions as for the fission rate above can be drawn: a standard sinus shape of the power is observed, with some small peaks above and below the graphite stringer.

Figure 23 compares the integrated radial and axial power profiles between the fresh core and the core at 375 days. Because of the low burnup at 375 days, the power profiles are consistent. The same conclusion is drawn when inserting zone-dependent inventory from the loop model (Section 3.3); no impact on the power profile can be observed.

While the nominal full core model assumed a constant temperature of 911 K for both the graphite structure and the fuel salt, the MELCOR team provided temperature profiles based on the power profiles of the nominal model at 375 days (Figure 22). MELCOR predicted the fuel salt temperature (which implies a fuel salt density change, see Section 5.3) to increase from 910.5 K at the bottom of the core to 937.7 K at the top of the core. The graphite temperature varied between 912.3 and 937.7 K. The impact of this temperature update was

negligible, as illustrated in Figure 24. The discretization in this plot is different since the power profiles in this figure are following the discretization used in the MELCOR model. Given that the impact was negligible, no further iterations between the power profiles and temperature distributions were deemed necessary.

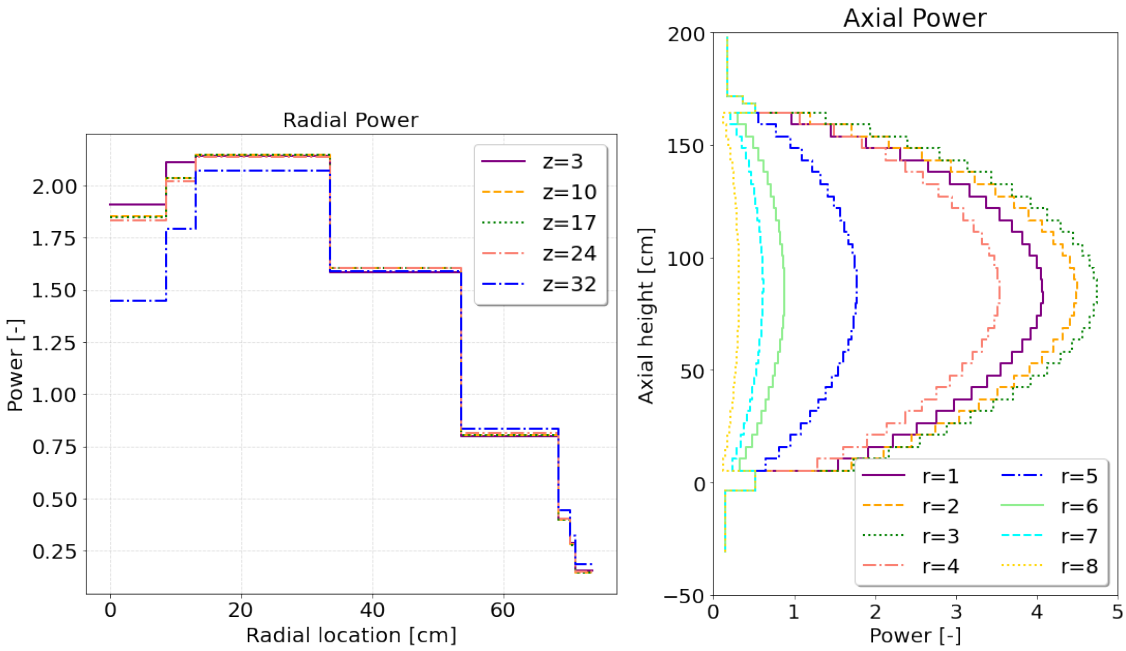


**Figure 22. Normalized axial and radial power profiles.**

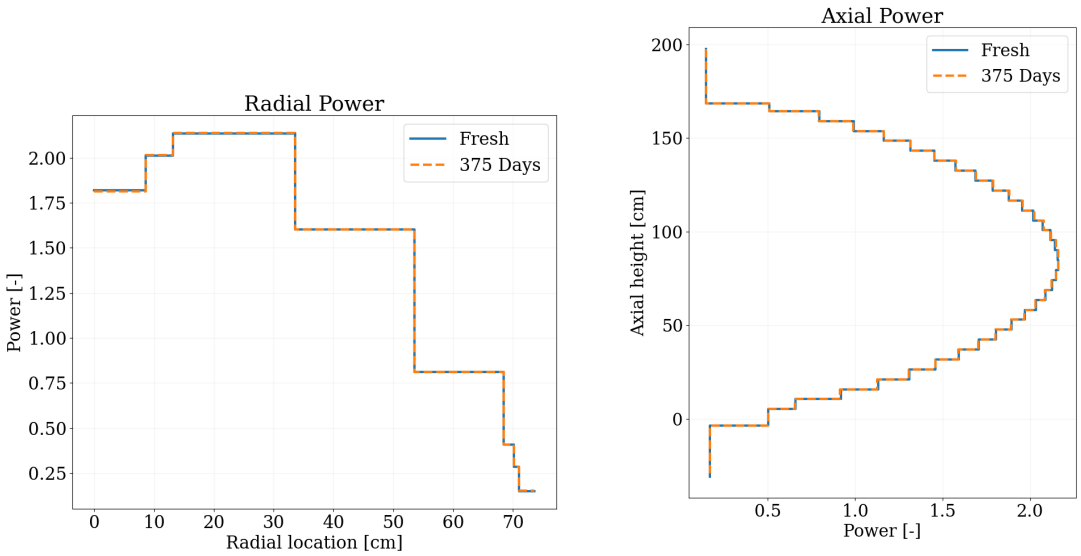


**Figure 23. Integrated, normalized radial and axial power profiles for the fresh core and the core at 375 days.**

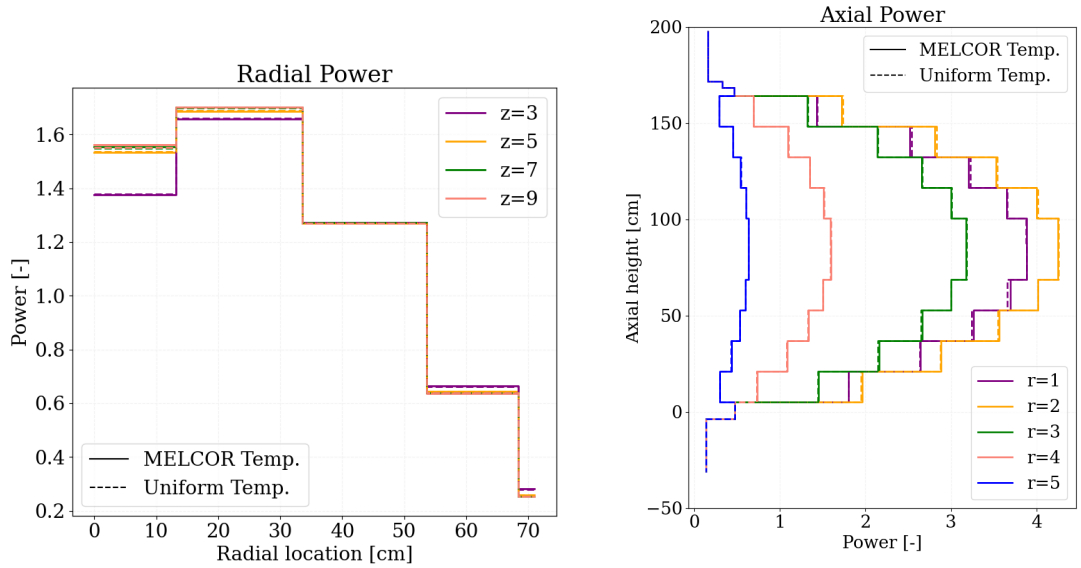


**Figure 24. Normalized axial and radial power profiles compared between static temperatures and a temperature distribution.**

### 5.3 REACTIVITY ANALYSIS

The $\beta_{\text{eff}}$ is an important kinetics parameter because it is crucial for reactivity control. In a circulating fuel reactor such as MSRE, DNP drift causes some of the delayed neutrons to be born outside the core. Therefore, the $\beta_{\text{eff}}$ of a core with circulating fuel is usually lower than for the same core with static conditions; in fact, the impact of DNP on $\beta_{\text{eff}}$ is dependent on the flow rate.

The $\beta_{\text{eff}}$ presented in this study is at static condition, and it is calculated using the *k-ratio* method [28]:

$$\beta_{eff} = 1 - \frac{k_p}{k}. \tag{10}$$

It is computed by using the ratio of the multiplication factor without delayed neutrons $k_p$ (prompt multiplication factor) to the multiplication factor with both prompt and delayed neutrons $k$. Thus, an additional eigenvalue calculation with only prompt neutrons is performed with TRITON-KENO. For both the fresh core and the core at 375 days, a $\beta_{\text{eff}}$ of approximately 700 pcm was found (Table 6). This value is in good agreement with a reported calculated value analytically for a MSRE steady-state operation [29].

**Table 6. $\beta_{\text{eff}}$, reactivity coefficients and $^{135}$Xe poisoning**

| Parameter | Fresh core | 375 days | Reported |
|---|---|---|---|
| $\beta_{\text{eff}}$ [pcm] | 704 ± 14 | 697 ± 22 | 666.1 [29] |
| $\alpha_{graphite}$ [pcm/K] | -5.13 ± 0.05 | -4.83 ± 0.07 | -4.68 [30] |
| $\alpha_{salt}$ [pcm/K] | -8.27 ± 0.12 | -8.28 ± 0.12 | -8.46 ± 1.26 [30] |
| $^{135}$Xe worth [pcm] | N/A | -337.17 ± 13.84 | -270 [31] |

The most important temperature-dependent reactivity feedback in the MSRE originates from the fuel salt and the graphite structure. Therefore, the reactivity coefficients for these materials ($\alpha_{graphite}$ and $\alpha_{salt}$) were calculated. They indicate by how much change the materials' temperature affects the core reactivity as a result of changes in the neutron absorption reaction rates and neutron leakages. It is noted that this reactivity analysis focuses on short-term temperature effects. Long-term effects such as the expansion of the reactor vessel or the swelling of the graphite moderator that can have an impact on reactivity are not considered.

For the calculation of $\alpha_{graphite}$, reactivity calculations with TRITON-KENO were performed for a range of models in which the temperature of the graphite structure was varied between 400 to 1,400 K. Taking the derivative of the fitted reactivity curve as a function of temperature yields the reactivity coefficient. The same approach was followed for $\alpha_{salt}$. However, a temperature change in the liquid fuel salt implies a change in the fuel salt density, which was considered by using a fuel salt expansion coefficient of $-1.18 \times 10^{-4}/^{o}$F [9].

Figure 25 shows the linear behavior of the reactivity for both the graphite temperature and the fuel salt temperature/density. Table 6 shows the gradients of the curves $\alpha_{graphite}$ and $\alpha_{salt}$. Both reactivity coefficients are clearly negative. For the fuel salt, there are two major drivers: increasing absorption in $^{238}$U with higher temperatures due to resonance broadening, and the decreasing fuel density, i.e. less $^{235}$U, with increasing temperatures (e.g., a factor of 0.9 at 1,400 K). Higher temperatures also cause a spectrum shift to higher energies, which is increasing neutron leakage.

$\alpha_{graphite}$ is slightly less negative at 375 days compared to that of the fresh core because of the smaller concentrations of graphite impurities in the 375 day core (e.g., the $^{10}$B density in the 375 day core is only 62% of the that in the fresh core). In contrast, $\alpha_{salt}$ shows a consistent value for both cores; the impact of fission products do not seem to make a large difference, and less than 0.5% of $^{238}$U was consumed, so the

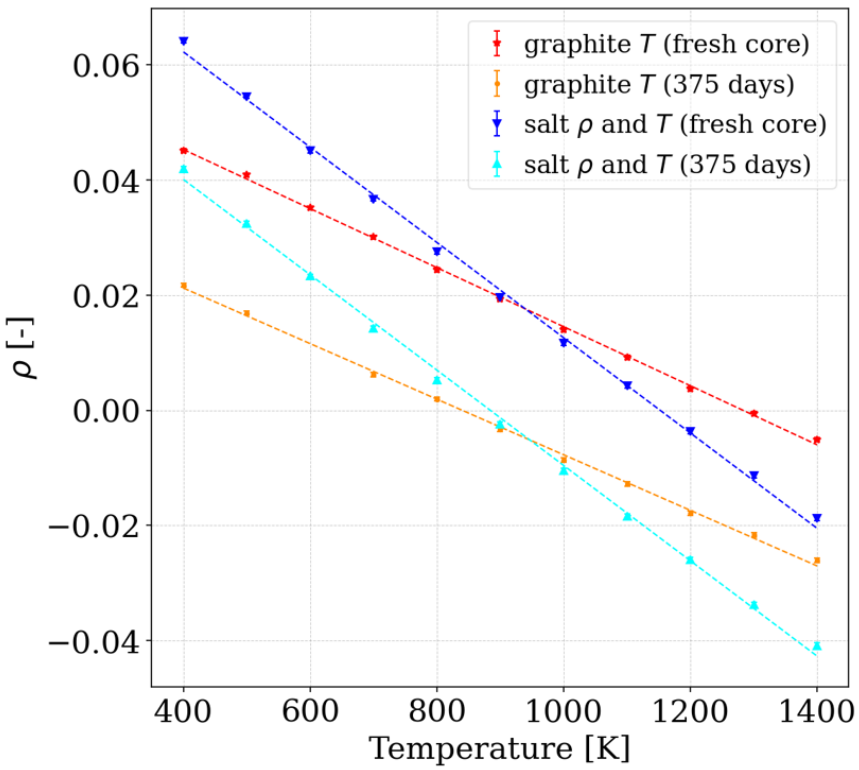


**Figure 25. Reactivity as function of the salt temperature (with implied density change) and the graphite temperature.**

impact of resonance broadening is not significantly changed. The results for both $\alpha_{graphite}$ and $\alpha_{salt}$ are in good agreement with those measured in 1960s during the zero-power physics experiment [30, 32].

The concentration of $^{135}$Xe in the fuel salt is controlled by the stripping efficiency of the OGS, and it impacts the xenon worth of the core. The analysis in Section 4 shows that an approximately constant concentration of $^{135}$Xe in the fuel salt is obtained after a few days of operation as a result of the continuous production of $^{135}$Xe as fission product, as well as the continuous removal through the OGS and decay. In theory, there is another effect in which $^{135}$Xe is transferred to the graphite structure. However, this is not considered in this study. The $^{135}$Xe poisoning found in the MSRE with the applied nuclide removal rates reduces the core reactivity by about 337 pcm.

## 6. ANALYSIS OF LOCATION-DEPENDENT NUCLIDE INVENTORY

The flowing fuel salt or fuel slug as it travels through the whole MSRE primary salt loop is modeled by ORIGEN, taking into account the transit time of salt in each region (Table 2), using the pregenerated system-average composition at 375 days and one-group cross sections from the axial slice core model, and also the axial flux profile generated from the 3D core model at 375 days (see Section 3.3). The MSRE primary loop is divided into 9 regions (Figure 7), and the core (region 1) is further divided into 30 axial zones.

### 6.1 ESTABLISHING "CONVERGED" LOCATION-DEPENDENT INVENTORY

ORIGEN is used to determine location-dependent inventory over several loops to reach a convergence of nuclide densities in the individual regions. Technically speaking, true convergence—in which $\frac{dN_i}{dt} = 0$ in each region—is not possible given the constant production and depletion of certain nuclides. While long-lived nuclides will slowly accumulate (e.g., salt-seeking fission and decay products such as Nd) or be removed (e.g., depletion of $^{235}$U), short-lived nuclides will oscillate around an equilibrium. Long-lived and short-lived nuclides are considered here with respect to the transit time of the fuel salt through the loop, which is only 25.2 seconds for the MSRE.

For the short-lived nuclides, approximate convergence conditions can be reasonably established as some threshold by which $N_i$ or $\frac{dN_i}{dt}$ no longer changes significantly at a given point in the loop compared to its total value:

$$\frac{1}{N_i}\left|\frac{dN_i}{dt}\right| < \text{threshold}, \tag{11}$$

or

$$\frac{1}{N_i}\left|\frac{d^2N_i}{dt^2}\right| < \text{threshold}. \tag{12}$$

Setting threshold criteria based on Eqs. (11) or (12) depends on the application. For instance, modeling DNP drift phenomena requires knowledge of $N_i$, so (11) would be used. However, the nuclide buildup in the HX (plate-out) relies on $\frac{dN_i}{dt}$ and would therefore more appropriately adhere to the threshold conditions of Eq. (12).

For example, this condition is applied to the change in concentration of nuclide $i$ at the HX, where $\phi = S_i = \lambda_{i,l,rem} = 0$, for a burnup time of 10 days. Applying the loop convergence criteria to the analytical form of the Bateman Equation, Eq. (1), we obtain

$$\frac{1}{N_i}\left|\sum_{j\neq i}^{M}\left(l_{ij}\lambda_j\right)\frac{dN_j}{dt} - \lambda_i\frac{dN_i}{dt}\right| < \text{threshold}. \tag{13}$$

ORIGEN integrates Eq. (1) to output total nuclide values, $N_i$, thus discretizing time steps (i.e., $dt = t_j - t_{j-1}$) in terms of the loop transit time such that with $dt \equiv 1$, Eq. (12) reduces to

$$\frac{N_{i,j} - 2N_{i,j-1} + N_{i,j-2}}{N_{i,j}} < \text{threshold}. \tag{14}$$

Applying the same discretization scheme to Eq. (11), we see

$$\frac{N_{i,j} - N_{i,j-1}}{N_{i,j,eq}} < \text{threshold}. \tag{15}$$

Note that the number of loops needed to satisfy these threshold criteria depends on the system's level of burnup as the initial value, $N_{i,0} \equiv N_{i,eq}$, where $N_{i,eq}$ is defined by Eq. (5), as obtained from the TRITON-KENO core slice calculation. In other words, for lower burnup, where $N_{i,eq}$ is relatively small, establishing converged conditions requires more iterations (i.e., transits through the loop) than at higher burnup for a given threshold.

The change in $\frac{dN_i}{dt}$ with respect to iteration number is shown in Figure 26 for several nuclides. For iterations greater than 5, the relative change in $\frac{dN_i}{dt}$ drops below 1%, which is an adequate threshold for most purposes. A more specific example is provided in Figure 27, which shows the nuclide density of the short-lived fission product $^{137}$I at the bottom of the graphite structure. $^{137}$I has a half life of 24.5 seconds, which is close to the loop transit time. The density of approximately $1.3 \cdot 10^{-13}$ atoms/b-cm at $t = 0$ corresponds to the system-average density. After approximately 6 transits/iterations through the loop, the density is converged to a lower value. To be slightly more conservative, the final location-dependent inventory was obtained using 10 transits through the MSRE loop. Those 10 transits of 25.2 seconds only minimally change the overall burnup or inventory of the fuel salt.

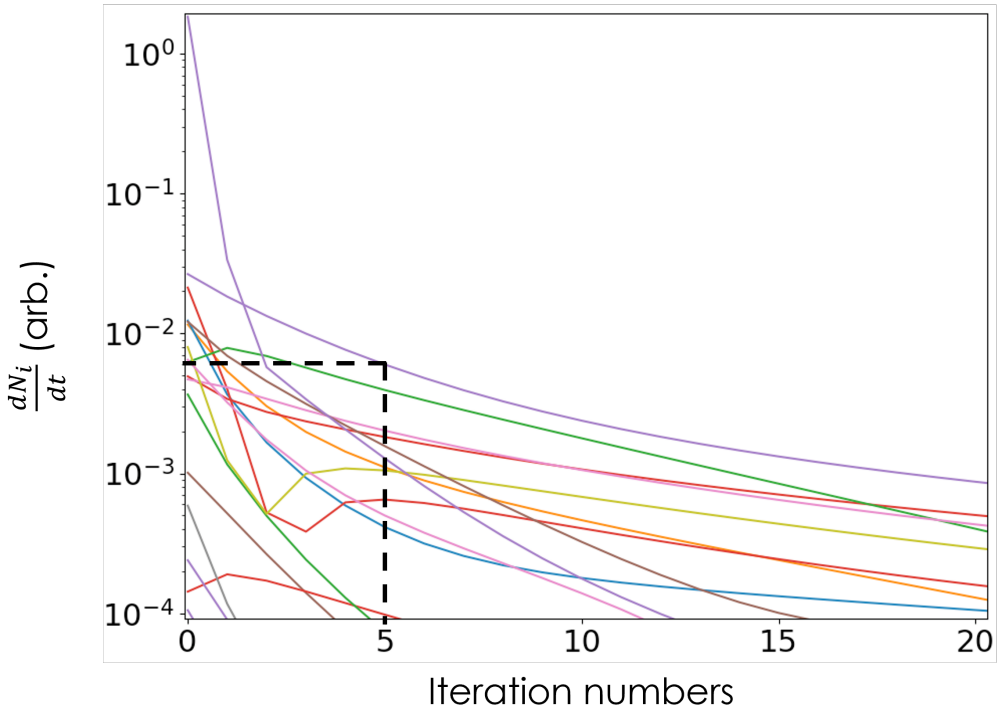


**Figure 26. Change of the loop inventory (random selection of nuclides) at the HX as a function of transits through the loop.**

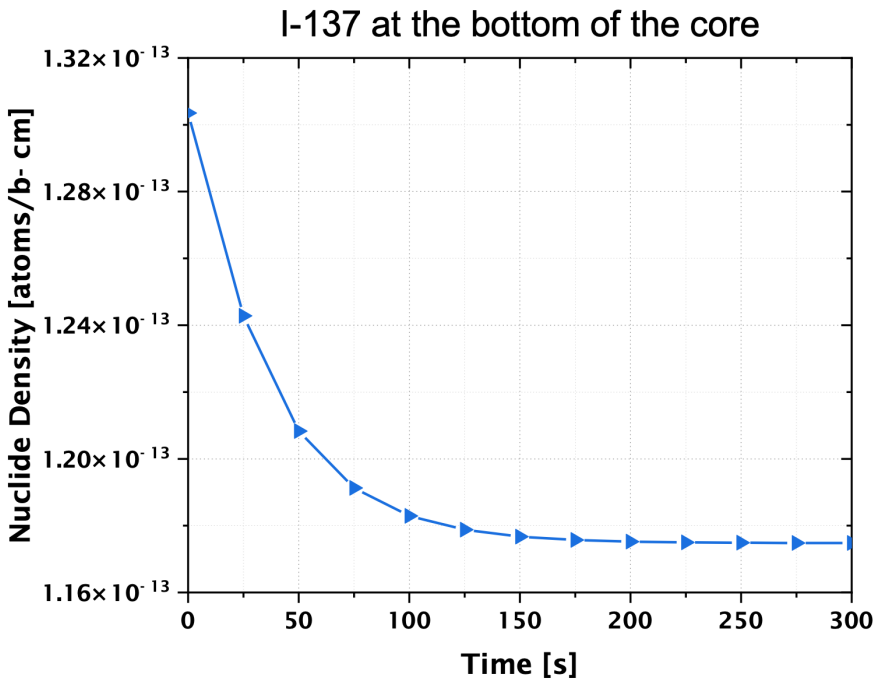


**Figure 27. Density of $^{137}$I at the bottom of the graphite structure as a function of time, corresponding to multiple transits through the loop (i.e., multiple iterations).**

### 6.2 ANALYSIS OF LOCATION-DEPENDENT INVENTORY

Based on 10 transits through the loop as calculated with ORIGEN, location-dependent inventory was obtained. For long-lived nuclides, the densities are constant over all regions in the loop. However, for short-lived nuclides, a spatial distribution can be observed. Figure 28 presents the nuclide density of $^{137}$I at different locations in the loop. The $^{137}$I density of a fuel slug is increasing, while the slug is moving up through the core because $^{137}$I is continuously built up as fission product. In the loop outside the core, or the regions with zero flux, the $^{137}$I density decreases as a result of the short half life ($t_{1/2}$ = 24.5 s). The developed equilibrium is once again visible by region 9, the lower head, having about the same density as the lowermost region of the core (region 1). As an additional example, Figure 29 presents the density of relevant DNPs in the reactor vessel.

When generating the inventory and decay heat file for MELCOR, the data for multiple elements are lumped together to align with MELCORs 14 element classes:

- XE : He, Ne, Ar, Kr, Xe, Rn, H, N
- CS : Li, Na, K, Rb, Cs, Fr, Cu
- BA : Be, Mg, Ca, Sr, Ba, Ra, Es
- I2 : F, Cl, Br, I, At
- S : S, Po
- RE : Re, Os, Ir, Pt, Au, Ni
- V : V, Cr, Fe, Co, Mn, Ta, W
- MO : Mo, Tc, Ru, Rh, Pd, Ag, Ge, As, Sn, Sb

- NB : Nb,Zn, Cd, Se,Te
- CE : Ti, Zr, Hf, Ce, Th, Pa, Np, Pu, C
- LA : Al, Sc, Y, La, Ac, Pr, Nd, Pm, Sm, Eu, Gd, Tb, Dy, Ho, Er, Tm, Yb, Lu, Am, Cm, Bk, Cf
- UO2 : U
- CD : Hg, Ga, In
- AG : Pb, Tl, Bi
- BO2 : B, Si, P

Due to the lumping of many nuclides in these classes, the masses and consequentially the decay heat of these element classes varied only negligibly between the different regions. Not considering the V class that only had negligible masses of less than $1 \cdot 10^{-15}$ kg in all individual regions, the largest standard deviation was observed with 0.63% for the Xe class, followed by the Re class (0.17%) and the Nb class (0.04%). The standard deviation of all other classes was below 0.01%. It was therefore concluded that for MSRE with the short transit time, the system-average inventory provides an appropriate approximation for all regions in the core as long as the different nuclide removal mechanisms are considered.

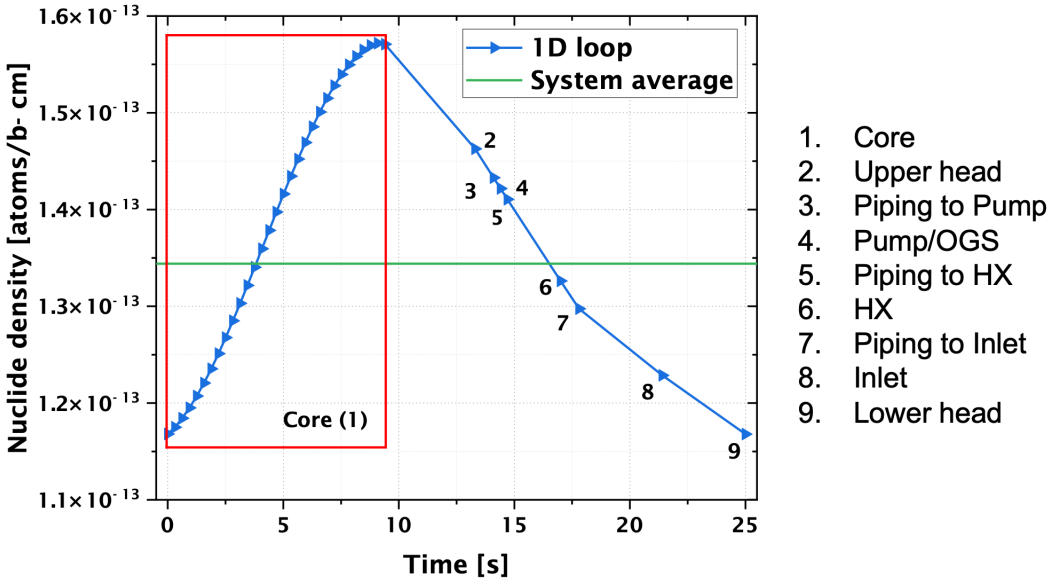


**Figure 28. Density of $^{137}$I in the different locations in the loop.**

### 6.3 DECAY HEAT ANALYSIS

While the TRITON-KENO core slice model only resulted in an average core+loop inventory and decay heat assessment, the ORIGEN loop calculation resulted in location-dependent inventory and also decay heat in the primary salt loop. Figure 30 shows that while the major part of the decay heat is naturally generated by the core (i.e., the region in the reactor vessel with the graphite structure), regions near the core (the upper head, the inlet, and the lower head) have noticeable contributions to the total decay heat. The estimates of decay heat at other components in the loop can also be used to inform potential further decay heat removal needs.

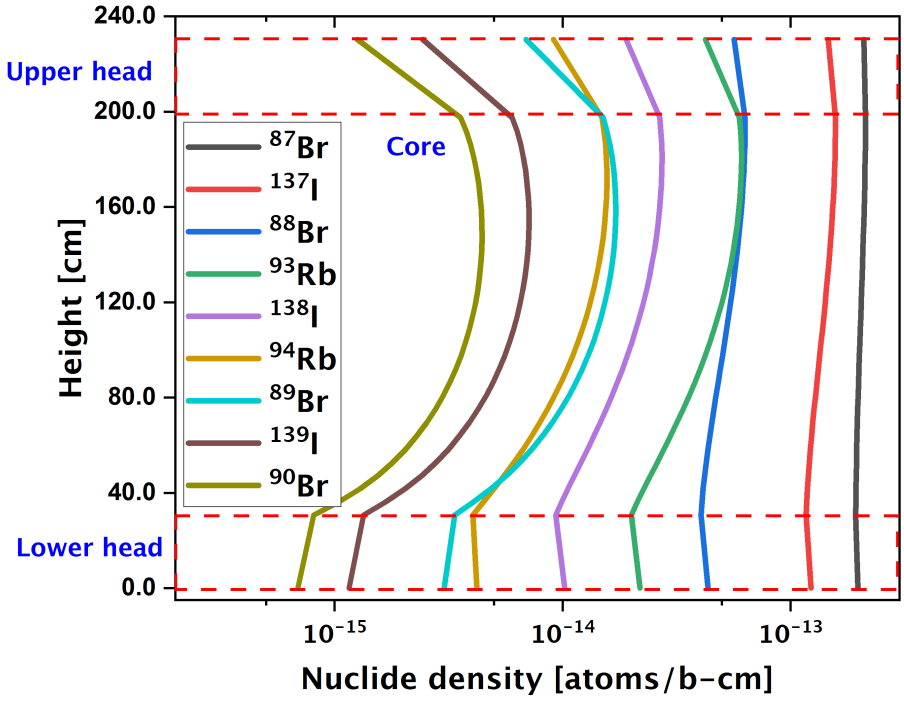


**Figure 29. Spatial delayed neutron precursors distribution.**

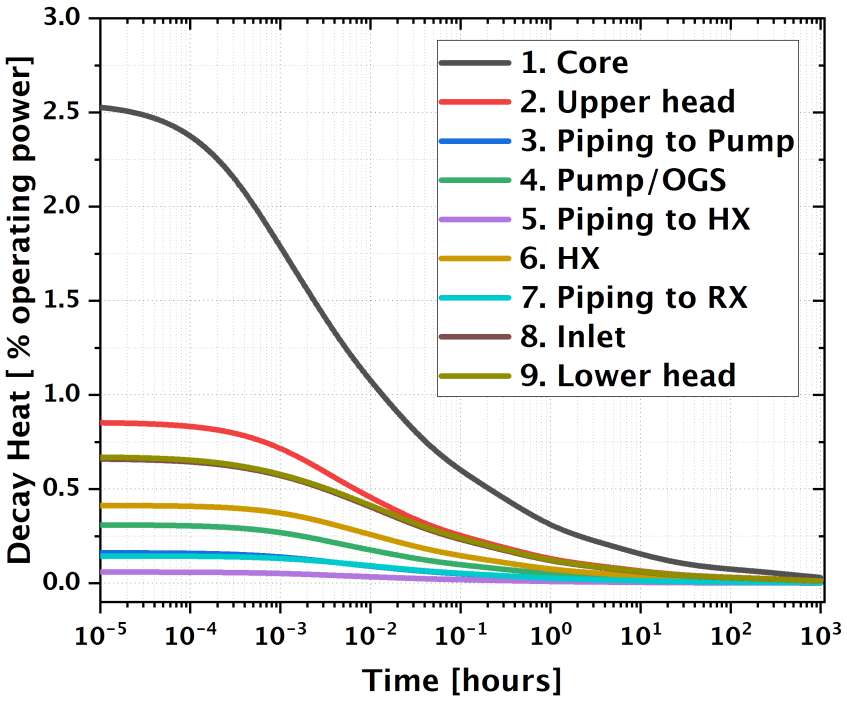


**Figure 30. Decay heat after 375 days of operation in each region of the loop.**

## 7. SUMMARY AND OUTLOOK

In this work the application of SCALE for the analysis of MSRs was demonstrated, with focus on obtaining an accurate estimation of nuclide inventories for long (days-to-years) and short (seconds-to-hours) time scales considering the key phenomena associated with flowing fuel and nuclide removal from the fuel. Both system-average fuel inventory and the inventory in different regions in the loop was determined. Based on the estimated inventory, the decay heat was calculated, and full core calculations were performed to determine power profiles and reactivity coefficients.

The calculation of system-average inventory, i.e. average fuel salt compositions of the core and loop, was performed using recent enhancements in SCALE's reactor physics sequence, TRITON. TRITON was used to calculate the system-average inventory at the end of MSRE's operation under consideration of continuous nuclide removal from the fuel salt through two paths: noble gas removal through the off-gas system, and noble metal plating out at the heat exchanger. The prediction of the nuclide inventory in the off-gas system was improved by considering continuous removal of the gas into a charcoal filter after an initial hold-up time. Because TRITON tracks the accumulation in each region, it was possible to estimate the decay heat for the fuel salt, the off-gas system, and the plated out material.

The calculation of location-dependent inventory in the system showed only small changes of the densities of specific nuclides over the different regions. Meaningful differences in concentrations were only found for short-lived nuclides with respect to the short loop transit time in the MSRE, which is intuitive. It was demonstrated that inventory and decay heat can be assessed in individual regions, but the location-dependence was found to be negligible when considering that MELCOR considers inventory and decay heat in element classes for which the data of many nuclides are summed together.

The full core calculations with TRITON-KENO resulted in power profiles that followed expected shapes when considering the air-filled control rod channels in the center of the core. The consideration of spatially dependent inventory in the core and temperature distributions provided by the MELCOR team was found to have negligible impacts on the power profiles. Given the small temperature change over the core, the use of constant temperatures and system-average inventory was found to be sufficient. Strongly negative temperature reactivity coefficients were found for the graphite and for the fuel salt for both a fresh-fueled MSRE core and the core at end of operation. For the fuel salt, it was necessary that the calculations consider that a temperature change of the fuel salt induces a density change. This also results in a negative fuel temperature reactivity feedback (approximately -8 pcm/K) with an absolute value of about twice as much as in a typical solid-fueled reactor.

The results obtained with SCALE were post processed to provide the MELCOR team with the core inventory and decay heat of the system, as well as individual regions in the loop, a zone-wise power profile, and temperature feedback coefficients for the simulation of accident scenarios concerning the spill of molten salt into the reactor containment [33].

Future work will include the integration of SCALE/ORIGEN into MELCOR so that MELCOR can calculate nuclide decay during accident scenarios instead of relying on pre-calculated and tabulated data. The integration of DNP drift model is of interest for transient calculation. The integration of such a model into MELCOR that allows a higher fidelity model than the standard 6-group DNP approach is simplified by the coupling with ORIGEN. Future work will also involve further improvements to TRITON's nuclide feed and removal capability and the generation of ORIGEN reactor libraries for MSRE to allow rapid inventory calculations (within seconds instead of hours).

## REFERENCES


[1] US NRC, "NRC Non-Light Water Reactor (Non-LWR ) Vision and Strategy, Volume 3: Computer Code Development Plans for Severe Accident Progression, Source Term, and Consequence Analysis," Tech. Rep. ML20030A178, Rev. 1, U.S. Nuclear Regulatory Commission, Rockville, MD, 2020.

[2] L. L. Humphries, B. A. Beeny, F. Gelbard, D. L. Louie, J. Phillips, R. C. Schmidt, and N. E. Bixler, "MELCOR Computer Code Manuals Vol. 1: Primer and Users' Guide Version 2.2.18019," Tech. Rep. SAND2021-0726 O, Sandia National Laboratories, Albuquerque, NM, 2021.

[3] S. E. Skutnik and W. A. Wieselquist, "Assessment of ORIGEN Reactor Library Development for Pebble-Bed Reactors Based on the PBMR-400 Benchmark," Tech. Rep. ORNL/TM-2020/1886, Oak Ridge National Laboratory, Oak Ridge, TN, 2021.

[4] E. Walker, S. E. Skutnik, W. A. Wieselquist, A. Shawn, and F. Bostelmann, "SCALE Modeling of the Fast-Spectrum Heat Pipe Reactor," Tech. Rep. ORNL/TM-2021/2021, Oak Ridge National Laboratory, Oak Ridge, TN, 2021.

[5] F. Bostelmann, C. Celik, R. F. Kile, and W. A. Wieselquist, "SCALE Analysis of a Fluoride Salt Cooled High Temperature Reactor in Support of Severe Accident Analysis," Tech. Rep. ORNL/TM-2021/2273, Oak Ridge National Laboratory, Oak Ridge, TN, 2022.

[6] H. G. Macpherson, "The Molten Salt Reactor Adventure," *Nuclear Science and Engineering*, vol. 90, no. 4, pp. 374–380, 1985.

[7] US NRC, "Pre-Application Activities for Advanced Reactors." https://www.nrc.gov/reactors/new-reactors/advanced/licensing-activities/pre-application-activities.html. Accessed: 2022-09-07.

[8] M. Fratoni, D. Shen, G. Ilas, and J. J. Powers, "Molten Salt Reactor Experiment Benchmark Evaluation," Tech. Rep. DOE-UCB-8542, 16-10240, University of California, Berkeley, 2020.

[9] D. Shen, M. Fratoni, M. Aufiero, A. Bidaud, J. J. Powers, and G. Ilas, "Zero-Power Criticality Benchmark Evaluation of the Molten Salt Reactor Experiment," *Proceedings of PHYSOR 2018, Cancun, Mexico, April 22–26*, pp. 4012–4024, 2018.

[10] D. Shen, G. Ilas, J. J. Powers, and M. Fratoni, "Reactor Physics Benchmark of the First Criticality in the Molten Salt Reactor Experiment," *Nuclear Science and Engineering*, 2021.

[11] W. A. Wieselquist, R. A. Lefebvre, and M. A. Jessee, "SCALE 6.2.4 User Manual," Tech. Rep. ORNL/TM-2005/39, Oak Ridge National Laboratory, Oak Ridge, TN, 2020.

[12] B. R. Betzler, J. J. Powers, and N. Brown, "Implementation of Molten Salt Reactor Tools in SCALE," *Proceedings of M&C 2017, Jeju Island, South Korea, May 16–20*, 2017.

[13] B. R. Betzler, K. B. Bekar, W. A. Wieselquist, S. W. Hart, and S. G. Stimpson, "Molten Salt Reactor Fuel Depletion Tools in SCALE," *Proceedings of Global 2019, Seattle, WA, September 22–27*, 2019.

[14] B. R. Betzler, J. J. Powers, J. L. Peterson-Droogh, and A. Worrall, "Fuel Cycle Analysis of Thermal and Fast Spectrum Molten Salt Reactors," *Proceedings of GLOBAL 2017, Seoul, South Korea, September 24–29*, 2017.

[15] B. R. Betzler, J. J. Powers, and A. Worrall, "Molten Salt Reactor Neutronics and Fuel Cycle Modeling and Simulation with SCALE," *Annals of Nuclear Energy*, vol. 101, pp. 489–503, 2017.

[16] P. Jr. Vicente Valdez, B. R. Betzler, W. A. Wieselquist, and M. Fratoni, "Modeling Molten Salt Reactor Fission Product Removal with SCALE," Tech. Rep. ORNL/TM-2019/1418, Oak Ridge National Laboratory, Oak Ridge, TN, 2020.

[17] J. W. Bae, B. R. Betzler, and A. Worrall, "Molten Salt Reactor Neutronic and Fuel Cycle Sensitivity and Uncertainty Analysis," *Transactions of American Nuclear Society*, vol. 121, pp. 1339–1342, 2019.

[18] J. W. Bae, B. R. Betzler, and W. A. Wieselquist, "Solving Advection Problems with Isotopic Evolution with SCALE/ORIGEN," *Proceedings of M&C 2021, Virtual Meeting*, pp. 2133–2144, 2021.

[19] F. Bostelmann, S. E. Skutnik, E. Walker, G. Ilas, and W. A. Wieselquist, "Modeling of the Molten Salt Reactor Experiment with SCALE," *Nuclear Technology*, vol. 208, no. 4, pp. 603–624, 2022.

[20] W. A. Wieselquist and R. A. Lefebvre, "SCALE 6.3.0 User Manual," Tech. Rep. ORNL/TM-SCALE-6.3.0, Oak Ridge National Laboratory, Oak Ridge, TN, 2021.

[21] M. Chadwick, M. Herman, P. Obložinský, M. Dunn, Y. Danon, A. Kahler, D. Smith, B. Pritychenko, G. Arbanas, R. Arcilla, R. Brewer, D. Brown, R. Capote, A. Carlson, Y. Cho, H. Derrien, K. Guber, G. Hale, S. Hoblit, S. Holloway, T. Johnson, T. Kawano, B. Kiedrowski, H. Kim, S. Kunieda, N. Larson, L. Leal, J. Lestone, R. Little, E. McCutchan, R. MacFarlane, M. MacInnes, C. Mattoon, R. McKnight, S. Mughabghab, G. Nobre, G. Palmiotti, A. Palumbo, M. Pigni, V. Pronyaev, R. Sayer, A. Sonzogni, N. Summers, P. Talou, I. Thompson, A. Trkov, R. Vogt, S. van der Marck, A. Wallner, M. White, D. Wiarda, and P. Young, "ENDF/B-VII.1 Nuclear Data for Science and Technology: Cross Sections, Covariances, Fission Product Yields and Decay Data," *Nuclear Data Sheets*, vol. 112, no. 12, pp. 2887–2996, 2011.

[22] P. N. Haubenreich and J. R. Engel, "Experience With the Molten-Salt Reactor Experiment," *Nuclear Applications and Technology*, vol. 8, no. 2, pp. 118–136, 1970.

[23] D. Shen, M. Fratoni, G. Ilas, and J. J. Powers, "Molten-Salt Reactor Experiment (MSRE) Zero-Power First Critical Experiment with U-235," Tech. Rep. MSRE-MSR-EXP-001, NEA/NSC/DOC(2006)1, Rev. 0, International Handbook of Reactor Physics Experiments, OECD/NEA, 2019.

[24] R. C. Robertson, "MSRE Design & Operations Report Part 1 Description of Reactor Design," Tech. Rep. ORNL-TM-728, Oak Ridge National Laboratory, Oak Ridge, TN, 1965.

[25] J. R. Engel, P. N. Haubenreich, and A. Houtzeel, "Spray, Mist, Bubbles, and Foam in the Molten Salt Reactor Experiment," Tech. Rep. ORNL-TM-3027, Oak Ridge National Laboratory, Oak Ridge, TN, 1970.

[26] R. J. Kedl and A. Houtzeel, "Development of a Model for Computing $^{135}$Xe Migration in the MSRE," Tech. Rep. ORNL-4069, Oak Ridge National Laboratory, Oak Ridge, TN, 1967.

[27] R. J. Kedl, "The Migration of a Class of Fission Products (Noble Metals) in the Molten-Salt Reactor Experiment," Tech. Rep. ORNL-TM-3884, Oak Ridge National Laboratory, Oak Ridge, TN, 1972.

[28] M. M. Bretscher, "Perturbation-Independent Methods for Calculating Research Reactor Kinetic Parameters," Tech. Rep. ANL/RERTR/TM-30, Argonne National Laboratory, Lemont, IL, 1997.

[29] P. N. Haubenreich, "Prediction of Effective Yields of Delayed Neutrons in MSRE," Tech. Rep. ORNL-TM-380, Oak Ridge National Laboratory, Oak Ridge, TN, 1962.

[30] B. E. Prince, S. J. Ball, J. R. Engel, P. N. Haubenreich, and T. W. Kerlin, "Zero-Power Physics Experiments on the Molten-Salt Reactor Experiment," Tech. Rep. ORNL-4233, Oak Ridge National Laboratory, Oak Ridge, TN, 1968.

[31] J. R. Engel and B. E. Prince, "The Reactivity Balance in the MSRE," Tech. Rep. ORNL-TM-1796, Oak Ridge National Laboratory, Oak Ridge, TN, 1967.

[32] B. E. Prince and J. R. Engel, "Temperature and Reactivity Coefficient Averaging in the MSRE," Tech. Rep. ORNL-TM-379, Oak Ridge National Laboratory, Oak Ridge, TN, 1962.

[33] US NRC/ORNL/SNL, "SCALE/MELCOR Non-LWR Source Term Demonstration Project – Molten Salt Reactor (MSR)." https://adamswebsearch2.nrc.gov/webSearch2/main.jsp?AccessionNumber=ML22255A214. Public presentation given on 2022-09-13.